Department of Agroecosystem Research
University of Bayreuth

M.Sc. Thesis in Global Change Ecology
in partial fulfillment of the requirements for the degree of

Master of Science

Modeling the response of water and carbon fluxes to atmospheric dryness in the land surface scheme JSBACH: Evaluating alternative process representations using multi-biome eddy covariance data

submitted by: Jürgen Knauer
matriculation number: 1288753

1. Supervisor: Prof. Dr. Christiane Werner
Department of Agroecosystem Research
University of Bayreuth

2. Supervisor: Prof. Dr. Martin Heimann
Department of Biogeochemical Systems
Max Planck Institute for Biogeochemistry

Bayreuth, 30th September 2014

Acknowledgements

This master thesis was conducted at the University of Bayreuth in collaboration with the Max Planck Institute for Biogeochemistry in Jena. I would like to thank my supervisors Prof. Christiane Werner and Prof. Martin Heimann for their support. I am very grateful to Dr. Sönke Zaehle for enabling this thesis, for his helpful guidance, and for his invaluable and unsolicited advice. Many thanks go to Prof. Markus Reichstein and the whole Department of Biogeochemical Integration for various discussions on the topic and the technical assistance provided. I am further grateful to all members of the Department of Agroecosystem Research at the University of Bayreuth for helpful comments on my work. I would also like to thank all my friends and my family for their support during the last six months.

Summary

Canopy conductance (G_c) is a key process in earth system models as it governs the transfer of carbon and water between the land surface and the lower atmosphere. Stomata themselves are sensitive to changes in environmental conditions and various approaches have been developed that aim for a robust yet simple representation of stomatal regulation applicable at the global scale. These models often differ in their response to atmospheric humidity which serves to induce stomatal closure to avoid excessive transpirational water losses in a dry atmosphere. In this study, the widely used "Ball-Berry" and "Leuning" type photosynthesis-stomatal conductance models are compared to a baseline model version which lacks a stomatal response to atmospheric humidity, as well as to alternative process representations based on the stomatal optimization theory and on the concept of transpiration supply and demand. All model variants were embedded in JSBACH, the land surface scheme of the MPI Earth system model. Model results of evapotranspiration (ET), gross primary productivity (GPP), and water use efficiency (WUE) were evaluated against eddy covariance measurements from 58 stations across multiple biomes and climatic conditions. Compared to the baseline model, all model versions showed significant improvements for ET and GPP for almost all plant functional types under conditions of non-limiting soil water availability, whereas WUE was generally overestimated. Model improvements occurred regardless of mean growing season VPD. Interestingly, differences of carbon and water fluxes between the alternative models were negligible for all plant functional types at the ecosystem scale. Thus, while the inclusion of a physiological response mechanism to atmospheric humidity is indispensable for all ecosystems, the functional type of such a response is of less importance for annual to decadal simulations at the global scale, despite regional and latitudinal differences. The outcome further suggests that current stomatal models could be improved by relating model parameters to environmental conditions or plant functional traits.

Contents

List of Tables

List of Figures

Symbols and abbreviations

Latin Letters

A_n	Net assimilation rate	µmol m^{-2} s^{-1}
$A_{n,0}$	Unstressed net assimilation rate	µmol m^{-2} s^{-1}
C_a	Atmospheric CO_2 concentration	µmol mol^{-1}
C_D	Transfer coefficient for momentum (=drag coefficient)	-
C_{DN}	Transfer coefficient for momentum (=drag coefficient) for neutral stability	-
C_h	Transfer coefficient for heat	-
C_i	Intercellular CO_2 concentration	µmol mol^{-1}
C_p	Specific heat of air	J mol^{-1} K^{-1}
C_s	CO_2 concentration at the leaf surface	µmol mol^{-1}
d	Zero-plane displacement height	m
D_0	Sensitivity parameter to vapor pressure deficit in the Leuning model	kPa
D_s	Leaf to surface vapor pressure deficit	kPa
E_c	Activation energy for CO_2	kJ mol^{-1}
E_g	Activation energy for Γ^*	kJ mol^{-1}
E_o	Activation energy for O_2	kJ mol^{-1}
ET	Evapotranspiration	mm d^{-1}
g	Gravitational acceleration	9.81 m s^{-2}
g_1	Slope parameter in coupled photosynthesis-stomatal conductance models	-
G_a	Aerodynamic conductance to water vapor	mol m^{-2} s^{-1}
G_c	Canopy conductance to water vapor	mol m^{-2} s^{-1}
$G_{c,0}$	Unstressed canopy conductance to water vapor	mol m^{-2} s^{-1}
g_0	Residual stomatal conductance	mol m^{-2} s^{-1}
GPP	Gross primary productivity	gC m^{-2} d^{-1}
g_s	Stomatal conductance to water vapor	mol m^{-2} s^{-1}
$g_{s,0}$	Unstressed stomatal conductance to water vapor	mol m^{-2} s^{-1}
h	Relative humidity	-
h_s	Relative humidity at the leaf surface	-
IWUE	Inherent water use efficiency	gC $kg^{-1}H_2O$ kPa
J	Electron transport rate	µmol m^{-2} s^{-1}
J_c	Rubisco-limited assimilation rate	µmol m^{-2} s^{-1}
J_e	RuBP-limited assimilation rate	µmol m^{-2} s^{-1}
J_i	light limited photosynthesis rate for C4 plants	µmol m^{-2} s^{-1}
J_i	light-limited assimilation rate (C4 photosnythesis)	µmol m^{-2} s^{-1}
J_m	Maximum electron transport rate	µmol m^{-2} s^{-1}
k	Von Kármán constant	0.41
K_c	Michaelis-Menten constant for CO_2	µmol m^{-2} s^{-1}
$K_{c,0}$	Michaelis-Menten constant for CO_2 at 25°C	µmol m^{-2} s^{-1}

K_o	Michaelis-Menten constant for O_2	mmol m^{-2} s^{-1}
$K_{o,0}$	Michaelis-Menten constant for O_2 at 25°C	mmol m^{-2} s^{-1}
k_s	PEPcase CO_2 specificity	mmol m^{-2} s^{-1}
O_i	Intercellular O_2 concentration	mmol mol^{-1}
p	Atmospheric pressure	kPa
q	Specific humidity	kg kg^{-1}
q_{sat}	Saturation specific humidity	kg kg^{-1}
R	General gas constant	8.314 J K^{-1} mol^{-1}
R_d	Dark respiration rate	µmol m^{-2} s^{-1}
Ri_b	Bulk Richardson number	-
R_n	Net radiation	W m^{-2}
T	Air temperature near the surface	K
T_g	Potential ground temperature	K
T_{max}	Maximum transpiration rate	mmol m^{-2} s^{-1}
T_{pot}	Potential transpiration rate	mmol m^{-2} s^{-1}
T_s	Potential air temperature at canopy height	K
T_{supply}	Transpiration supply rate	mmol m^{-2} s^{-1}
T_v	Vegetation temperature	K
u	Horizontal wind velocity	m s^{-1}
u_*	Friction velocity	m s^{-1}
V_{cmax}	Maximum carboxylation rate	µmol m^{-2} s^{-1}
VPD	Vapor pressure deficit	kPa
V_{pmax}	Maximum PEP carboxylation rate	µmol m^{-2} s^{-1}
WUE	Water use efficiency	gC $kg^{-1}H_2O$
z_0	Roughness length	m
z_s	Vegetation height	m

Greek Letters

β	Soil water stress factor	-
Δ	Specific humidity deficit	kg kg^{-1}
ϵ	Change of latent heat content relative to the change of sensible heat content of saturated air	kPa K^{-1}
Γ	CO_2 compensation point	µmol m^{-2} s^{-1}
γ	Psychrometric constant	kPa K^{-1}
Γ^*	CO_2 compensation point in the absence of dark respiration	µmol m^{-2} s^{-1}
Λ	Leaf area index	m^2 m^{-2}
λ	marginal water cost of plant carbon uptake	mol H_2O $mol^{-1}C$
λ_w	Latent heat of vaporization of water	J mol^{-1}
Ω	Decoupling coefficient	-
ρ	Air density	kg m^{-3}
Θ	Soil moisture content	m^3 m^{-3}
Θ_{crit}	Critical soil moisture content	m^3 m^{-3}
Θ_s	Curvature parameter for J_e	-
Θ_{wilt}	Soil moisture content at wilting point	m^3 m^{-3}

Abbreviations

BETHY	Biosphere-Energy-Transfer-Hydrology model
ECHAM	Atmosphere component of MPI-ESM
ECMWF	European Centre for Medium-Range Weather Forecasts
GCM	General circulation model
JSBACH	Land component of MPI-ESM
LAI	Leaf area index
LSM	Land surface model
MPI-ESM	Max Planck Institute Earth system model
NEE	Net ecosystem exchange
PFT	Plant functional type
USM	Unified stomatal model

1 Introduction

Stomata play a major regulating role in terrestrial water and carbon fluxes, as they control the exchange of both water vapor and carbon dioxide between the land surface and the atmosphere. High stomatal conductance (g_s) favors high photosynthetic rates and therefore gross primary productivity (GPP), but it is also accompanied by increased transpirational water losses under otherwise equal atmospheric conditions. An amplified water flux towards the atmosphere has consequences for the energy partitioning on the land surface as it increases the latent heat flux at the expense of the sensible heat flux. This effect lowers the Bowen ratio and surface temperature (Dirks and Hensen, 1999) with possible implications for mesoscale circulations in the atmospheric boundary layer (Mascart et al., 1991). Stomata themselves are sensitive to changes in their abiotic environment. A common observation is that stomata close under rising atmospheric CO_2 concentrations (Field et al., 1995). Under such conditions, leaf internal CO_2 concentrations and therefore photosynthesis can be maintained at the same level even if g_s decreases, while transpiration is reduced (Keenan et al., 2013). This leads to an increase in water use efficiency (WUE), a quantity describing the ratio of water loss to carbon gain, and a key ecosystem characteristic which links carbon and water cycling (Niu et al., 2011). In general, small changes in stomatal conductance are believed to have large effects on carbon and water fluxes, which feedbacks again with climate (Berry et al., 2010). This notion was confirmed by modeling studies using land surface models (LSMs) coupled to general circulation models (GCMs). Such model simulations have proposed that under doubled atmospheric CO_2 concentrations the effect of stomatal closure on temperature and precipitation would be similar in magnitude to the effects of CO_2 on radiation (Sellers et al., 1996). Reduced g_s and subsequently reduced transpiration rates have further been shown to be in accordance with an increase in continental runoff in the twentieth century (Gedney et al., 2006).
Although the focus of current research lies on the response of stomata to elevated atmospheric CO_2 concentrations and temperatures, stomata are known to respond to further environmental stimuli such as radiation, vapor pressure deficit (VPD), and soil water (e.g. Jarvis, 1976; Schulze, 1986), which makes the prediction of carbon and water fluxes under altered climate conditions more complex. Soil water availability for instance is already considered to be the main limiting factor for global plant growth (Nemani et al., 2003; Zhao and Running, 2010), and projections of climate change suggest an aggravation of the limiting role of droughts, as changes in precipitation patterns as well as an increase in air temperature are expected (Dai, 2011; Hartmann et al., 2013). Especially in subtropical regions, climate projections indicate a decrease in precipitation along with a decrease in soil moisture (Dai, 2011). However, droughts are not solely characterized by a deficit in atmospheric water supply (i.e. precipitation) but are further accompanied by changes in atmospheric demand (i.e. potential evapotranspiration) which is likely to increase along with temperature (Rind et al., 1990). Both soil and atmospheric drought impose limitations on plant growth by inducing decreases in stomatal conductance and photosynthesis (Zhou et al., 2013). Understanding the interplay between the response of photosynthesis and stomatal conductance to the combined effects of atmospheric and soil drought therefore remains a pressing challenge in climate and ecosystem models (Tuzet et al., 2003), especially since such models have been found to perform comparatively poor in regions characterized by seasonal water scarcity (Morales et al., 2005; Jung et al., 2007).

The predicted changes in environmental factors governing stomatal conductance in combination with the high sensitivity of global climate simulations to stomatal processes have emphasized the

need to include accurate process representations of canopy conductance in state of the art climate models (Berry et al., 2010). The vast majority of these models use empirical representations of stomatal conductance, which are based on the long-standing observation that g_s correlates with photosynthesis (Wong et al., 1979). One of the most popular representative of those models is the "Ball-Berry" model (Ball et al., 1987), which has proven very successful in large scale modeling approaches due to its simplicity (i.e. low number of free parameters) and its capability of giving accurate predictions of g_s at large spatial scales and under varying environmental conditions (Buckley and Mott, 2013). The model relates g_s to net assimilation rate (A_n), the leaf surface concentration of CO_2, and relative humidity. The original Ball-Berry model was modified several times (Leuning, 1990; Collatz et al., 1991; Aphalo and Jarvis, 1993; Leuning, 1995), and further empirical approaches have been proposed (Friend and Kiang, 2005), all of which differ with regard to the measure of atmospheric humidity employed and the mathematical function describing stomatal closure in response to a decrease in atmospheric humidity (Section 2.3).

One major drawback of empirical models, however, is that their parameters have no theoretical foundation, which hinders their prediction and interpretation across vegetation types or environmental conditions and restricts the model's predictive capability under changing environmental conditions (Gao et al., 2002; Medlyn et al., 2011). In this respect, modeling approaches using process-based formulations would be desirable, but remain unfeasible especially on regional and larger spatial scales due to an incomplete understanding of the underlying mechanisms (Damour et al., 2010; Buckley and Mott, 2013). Nevertheless, a promising alternative towards a more mechanistic representation of stomatal behavior are models which relate g_s to water flow in the soil-plant-atmosphere continuum. Such models make use of the concept of plant hydraulic architecture (Tyree and Ewers, 1991) and simulate water flow in dependence on the water potential difference between the soil and the leaf as well as the hydraulic conductance in its pathway (Damour et al., 2010). The resistance to water flow is primarily a function of plant characteristics such as path lengths and properties of water-conducting tissues (Zimmermann, 1978), and therefore requires detailed knowledge about plant hydraulic traits (Tyree and Ewers, 1991). Such an approach was implemented for a dynamic global vegetation model by Hickler et al. (2006), who modeled water flow based on resistances in the roots, xylem, and leaves and parameterized the formulations based on collected plant functional type-specific values extracted from the literature. Even though the model gave acceptable results, the formulations used in this model as well as in many other hydraulic models (e.g. Sperry et al., 1998; Tuzet et al., 2003), are comparatively complex and require much input information. A similar, but simplified process description (Knorr, 2000) represents plant hydraulic properties as a single parameter, which can be thought of as the maximum whole-plant hydraulic conductance. The model then simulates plant water loss as the lesser of a transpiration supply and demand rate (Federer, 1982), with the former being dependent on whole-plant water conductivity as well as soil moisture availability and the latter on atmospheric demand (Knorr, 2000). This approach is simple, but still suffers from parameter uncertainties, since information on plant hydraulic properties in the appropriate unit and for large spatial scales is rare.

A third major model family for stomatal conductance goes back to the theory of optimal stomatal behavior by Cowan and Farquhar (1977), who hypothesized that plants regulate stomatal aperture in such a way as to minimize water loss and maximize carbon gain over a given time interval, i.e. minimize the expression $(E - \lambda A_n)$, where A_n is net assimilation, E is transpiration, and λ is the marginal water cost of carbon to the plant. This theory has experienced increased popularity in recent years (Katul et al., 2009; Katul et al., 2010; Medlyn et al., 2011; Manzoni et al., 2011).

Based on the optimization theory, Katul et al. (2009) derived an expression of g_s which depends on the inverse square root of VPD, and showed that this expression appears consistent with the observed behavior of g_s with respect to VPD. Similarly, Medlyn et al. (2011) derived an equation, which they termed "the unified stomatal model", by combining the optimization theory with the Farquhar photosynthesis model (Farquhar et al., 1980). These approaches contain the marginal water cost of carbon (λ) as a parameter component, which offers new opportunities for explaining stomatal behavior to environmental stimuli. In contrast to the parameters in the Ball-Berry type models, λ is not an empirically fitted constant, but a biologically meaningful quantity, which is assumed to vary across plant functional types and environmental conditions (Manzoni et al., 2011; Medlyn et al., 2011). Since the derived equations remained simple, but include a predictable parameter, stomatal models based on the optimization theory appear to be a promising alternative to well-established and widely used empirical photosynthesis-stomatal conductance models for use in LSMs.

For this study, several stomatal conductance models were evaluated: (1) the Ball-Berry and (2) Leuning model, both empirical and widely used coupled photosynthesis-stomatal conductance models, (3) an alternative empirical model proposed by Friend and Kiang (2005), (4) a model combining empirical approaches with the stomatal optimization theory, the unified stomatal model (USM) (Medlyn et al., 2011), and (5) an approach based on plant hydraulic properties combined with the concept of transpiration supply and demand (Knorr, 2000). The main focus lied on the model performance under varying conditions of atmospheric drought, expressed as VPD, while water-stressed conditions were excluded. For that purpose, all models were implemented in JSBACH, the land surface scheme of the MPI Earth system model (Reick et al., 2013), which currently lacks a stomatal response to atmospheric dryness and thereby provides a baseline model. Models were evaluated against eddy covariance data from 58 stations covering multiple climate zones and biomes. Sites were aggregated into plant functional types according to the phenotype, photosynthetic pathway, and growth form of the vegetation. Site level runs were conducted for which LAI and photosynthetic capacity were adjusted to site conditions, and halfhourly model outputs of G_c, GPP, and ET were evaluated for different conditions of VPD. In a final step, global simulations were conducted to reveal spatial and latitudinal differences between the models. The study aims at assessing different process representations of stomatal conductance with regard to their capability of simulating observed fluxes of carbon and water fluxes for different ecosystems under varying conditions of atmospheric drought.

2 Materials and methods

2.1 The land surface model JSBACH

JSBACH (Raddatz et al., 2007; Reick et al., 2013; Schneck et al., 2013) is the land component of the Max Planck Institute Earth system model (MPI-ESM) (Giorgetta et al., 2013). Land physics components (surface radiation, energy balance, and heat transport) are inherited from the atmosphere model ECHAM5 (Roeckner et al., 2003). The biogeochemical components of JSBACH are in large parts based on the biosphere model BETHY (Biosphere-Energy-Transfer-Hydrology model) (Knorr, 2000). Soil hydrology is simulated with a five layer scheme (Hagemann and Stacke, 2014). The spatial units in the model are grid cells, which are again split into tiles to account for subgrid scale heterogeneity of vegetation cover (Reick et al., 2013). Each tile is associated with one plant functional type (PFT). JSBACH distinguishes 20 PFTs, which differ in their biochemical (e.g. maximum carboxylation rate, maximum electron transport rate, photosynthetic pathway), phenological (e.g. maximum LAI), and biogeophysical (e.g. vegetation height, albedo, surface roughness) attributes (Raddatz et al., 2007; Reick et al., 2013) (Tab. 1). The initial global distribution of vegetation types is prescribed on the basis of global land cover maps, but changes dynamically as vegetation in the model is subject to natural and anthropogenic land cover change (Reick et al., 2013). LAI is calculated with the phenology model LoGro-P (Raddatz et al., 2007), in which temperature and moisture dependent growth and shedding rates determine the annual course of LAI, which is constrained by a PFT-specific maximum value.

Tab. 1. PFT-specific parameter values

PFT[a]	V_{cmax} [μmol m^{-2}s^{-1}][b]	J_{max} [μmol m^{-2}s^{-1}][c]	vegetation height [m]	max. LAI [m^{2}m^{-2}]	T_{max} [mmol m^{-2}s^{-1}][d]	g_0 [mol m^{-2}s^{-1}][e]	g_1 [–][f]
TrEF	39.0	74.1	30	7	3.22	0.01	9.3
TrDF	31.0	58.9	30	7	3.22	0.01	9.3
TeBEF	61.4	116.7	15	5	1.29	0.01	9.3
TeBDF	57.7	109.7	15	6	2.57	0.01	9.3
CEF	62.5	118.8	15	5	1.93	0.01	9.3
TrH	30.0	300.0	0.3	3	3.86	0.08	3.0
TeH	78.2	148.6	0.3	3	3.86	0.01	9.3

[a] Plant functional type (TrEF = Tropical evergreen forest, TrDF = Tropical deciduous forest, TeBEF = Temperate broadleaf evergreen forest, TeBDF = Temperate broadleaf deciduous forest, CEF = Coniferous evergreen forest, TrH = C4 grassland, TeH = C3 grassland).

[b] V_{pmax} for C4 plants (TrH).

[c] value for C4 plants (TrH) represents k_s in mmol m^{-2} s^{-1} (Eq. A.2).

[d] values are based on Hickler et al. (2006).

[e] value for TrH from Collatz et al. (1992), all others from Ball et al. (1987).

[f] value for TrH from Collatz et al. (1992), all others from Ball et al. (1987). Values shown are the ones used for the Ball-Berry model; values were adjusted for the other model versions (section 2.3.6).

2.2 Current implementation of photosynthesis and stomatal conductance in JSBACH

In the current version of JSBACH (Version 2.0), G_c is insensitive towards changes in atmospheric humidity. This structural model deficiency was corrected by the implementation and evaluation of several models for stomatal conductance. While these model versions are based on the same photosynthesis model (section 2.2.1), the representation of stomatal conductance differs for each model.

2.2.1 Photosynthesis models

Net assimilation rate (A_n) is based on the photosynthesis models of Farquhar et al. (1980) for C3 plants and Collatz et al. (1992) for C4 plants. The Farquhar scheme simulates photosynthesis as limited by one of the two following biochemical processes: carboxylation rate limited by the activity of Rubisco (J_c), or carboxylation rate limited by the RuBP regeneration rate (J_e), which depends on the electron transport rate. A_n is given by the lesser of these two rates minus dark respiration (R_d):

$$A_n = \min(J_c; J_e) - R_d \tag{1}$$

with

$$J_c = V_{cmax} \frac{C_i - \Gamma^*}{C_i + K_c(1 + O_i/K_o)} \tag{2}$$

$$J_e = J \frac{C_i - \Gamma^*}{4(C_i + 2\Gamma^*)} \tag{3}$$

where V_{cmax} is the maximum carboxylation rate, C_i is the intercellular CO_2 concentration, Γ^* is the CO_2 compensation point in the absence of dark respiration, K_c and K_o are the Michaelis-Menten constants for CO_2 and O_2, O_i is the intercellular O_2 concentration, J is the electron transport rate, which depends on the rate of absorbed photosynthetic active radiation (Farquhar et al., 1980). R_d at 25°C is assumed to be proportional to V_{cmax} at 25°C. The temperature dependence of R_d is of the same form as Eq. B.1.

The temperature response function of Γ^* was changed from a linear to an exponential form, and the Rubisco kinetic parameters for the temperature responses of K_c and K_o were revised according to Bernacchi et al. (2001)(Appendix B). The values of V_{cmax} and J_{max} at the reference temperature of 25°C are prescribed for each PFT (Tab. 1). The temperature dependence of the two rates has the same form as those for the Michaelis-Menten constants (Eq. B.1, B.2), but includes an additional nitrogen scaling which accounts for variations of V_{cmax} and J_{max} within the canopy. Values for photosynthetic capacity of C4 plants (V_{pmax} and k_s at the reference temperature of 25°C) were changed according to Simioni et al. (2004).

2.2.2 Stomatal conductance

In the current version of JSBACH, net assimilation rate and stomatal conductance are first calculated for unstressed, i.e. non-water-limited conditions. The unstressed net assimilation rate $A_{n,0}$ is calculated from Eqs. 1-3 for C3 plants and from Eqs. A.1-A.3 for C4 plants, respectively. For that purpose, a prescribed intercellular CO_2 concentration C_i is used, which is set to $C_{i,0} = 0.87C_a$ for C3 plants and $C_{i,0} = 0.67C_a$ for C4 plants (Knorr, 2000), where C_a is the atmospheric CO_2 concentration and the subscript $_0$ denotes unstressed conditions with respect to soil moisture. The unstressed stomatal conductance $g_{s,0}$ can then be determined by solving the diffusion equation:

$$g_{s,0} = \frac{1.6A_{n,0}}{C_a - C_{i,0}} \tag{4}$$

where the factor 1.6 accounts for the higher diffusivity of the lighter water molecules compared to carbon dioxide. Under water stressed conditions, stomatal conductance g_s is derived by scaling the unstressed conductance from Eq. 4 with a water stress factor β, which is a simple function of

soil water content (section 4.4). Solving Eq. 4 for C_i and combining it with Eq. 2 and 3 gives two quadratic equations for J_c and J_e. A_n is then finally given by the minimum of the respective lesser solution of those quadratic equations (Knorr, 1997). All the calculations are conducted for three canopy layers. In all model versions, rates of A_n, R_d, and g_s at the canopy scale are calculated as the integral over the leaf area. Thus, canopy conductance G_c is given by:

$$G_c = \int_0^{\Lambda} g_s(l)\ dl \tag{5}$$

where Λ denotes the leaf area index (LAI) of the canopy, and dl its differential element.

2.3 Alternative stomatal conductance models implemented in JSBACH

2.3.1 The BETHY approach

This approach goes back to the stomatal conductance model as applied in the biosphere model BETHY by Knorr (2000) and to the work of Federer (1982). In this scheme, transpiration rate is assumed to be either limited by atmospheric demand (demand function) or by the supply of water and the hydraulic conductivity of plants (supply function) (Cowan, 1965; Federer, 1982). When the demand function exceeds the supply function, which occurs mostly under conditions of soil water scarcity or in a dry atmosphere, G_c is reduced by the ratio of the two functions (Fig. 12). The demand function is represented by the potential transpiration rate T_{pot}, which is here defined as the transpiration rate under given meteorological conditions, unlimited water supply, and maximum canopy conductance ($G_{c,0}$) as calculated from Eq. 4. T_{pot} strongly depends on the aerodynamic conductance (G_a), G_c, and on the saturation deficit of water in the air:

$$T_{pot} = \rho \frac{q_{sat}(T,p) - q}{\frac{1}{G_a} + \frac{1}{G_{c,0}}} \tag{6}$$

where ρ is air density, q is specific humidity and q_{sat} is saturation specific humidity at temperature T and pressure p. G_a in the model is calculated according to Eq. E.6. The supply function T_{supply} depends on the available soil water content in the root zone and on the maximum hydraulic conductivity (T_{max}) of vegetation and is computed as follows:

$$T_{supply} = \beta \cdot T_{max} \tag{7}$$

where β is a dimensionless soil stress factor as calculated in Eq. 15, and T_{max} is a PFT-specific maximum instantaneous transpiration rate, which represents the whole-plant hydraulic conductivity in this study, and which does not change with environmental conditions. T_{supply} however changes with soil moisture (Eq. 7). For this study, PFT-specific T_{max} values were determined based on values from the literature collected by Hickler et al. (2006) (Tab. 1). G_c is then given by:

$$G_c = \begin{cases} 0 & T_{supply} = 0 \\ G_{c,0} \cdot (T_{supply}/T_{pot}) & 0 < T_{supply} < T_{pot} \\ G_{c,0} & T_{supply} > T_{pot} \end{cases} \tag{8}$$

where $G_{c,0}$ is the unstressed canopy conductance as calculated in Eq. 4. A_n and C_i are calculated as in the standard model (section 2.2.2).

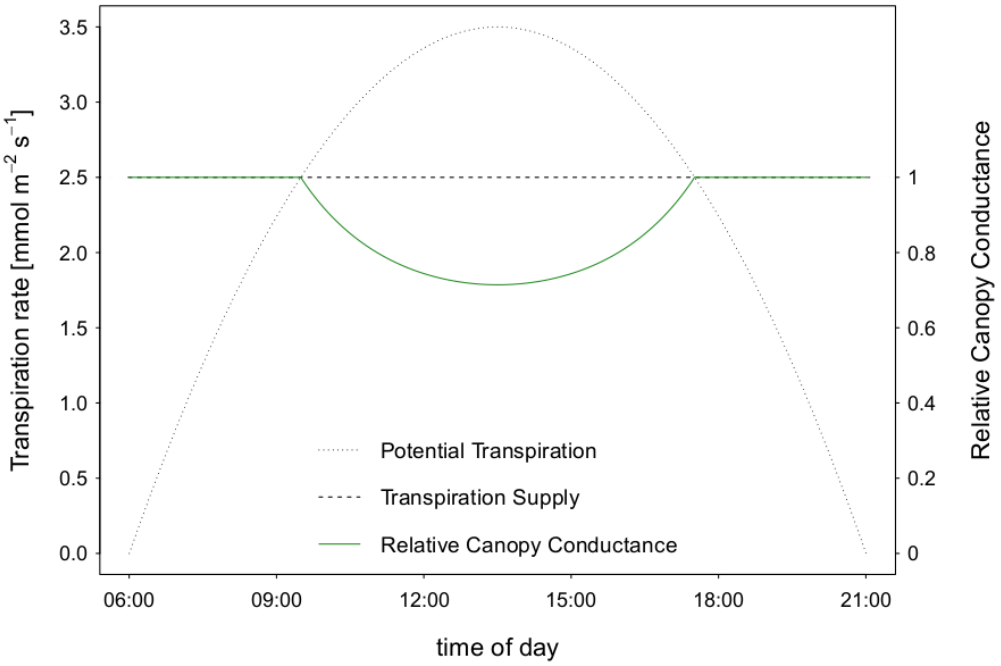

Fig. 1. Graphical representation of the BETHY model. G_c is lowered according to the ratio of T_{supply} to T_{pot} if transpiration is limited by T_{pot}. T_{supply} equals the maximum transpiration rate T_{max} if no soil water stress occurs, otherwise it is lowered by a water stress factor (Eq. 7). The situation as shown represents conditions of constant soil moisture throughout the day.

2.3.2 The Ball-Berry model

This approach is based on the observation that g_s is strongly correlated with A_n. Based on measurements of A_n and g_s under varying conditions of light, CO_2 concentration, temperature, and air humidity in a gas-exchange cuvette, Ball et al. (1987) derived the following formula for stomatal conductance:

$$g_s = g_0 + g_1 \frac{A_n h_s}{C_a} \tag{9}$$

where A_n is net assimilation rate, h_s is relative humidity at the leaf surface, and C_a is the mole fraction of CO_2 at the leaf surface. This equation describes a linear relationship between g_s and A_n, CO_2 concentration, and relative humidity (Ball et al., 1987), where g_0 is the residual conductance as A_n approaches 0, and g_1 is the slope of the function, which is in this study assumed to be constant in the absence of water stress.

The Ball-Berry model has often been criticized for its assumption that stomata respond to relative humidity. In fact, later studies suggested that stomata rather sense transpiration (Mott and Parkhurst, 1991) or its driving force VPD (Aphalo and Jarvis, 1991). Despite all criticism, the Ball-Berry model is widely used in GCMs (Buckley and Mott, 2013).

2.3.3 The Leuning model

Leuning (1995) developed a modified version of the Ball-Berry model, which is again based on a series of gas-exchange measurements on individual leaves and data extracted from the literature.

He replaced C_a with $(C_a - \Gamma)$ (Leuning, 1990) and the relative humidity term with an inverse hyperbolic response function of the leaf-to-surface vapor pressure deficit (D_s), which goes back to Lohammar et al. (1980). The revised model is given by:

$$g_s = g_0 + g_1 \frac{A_n}{(C_a - \Gamma)(1 + D_s/D_0)} \tag{10}$$

where Γ is the CO_2 compensation point, and D_0 is an empirically fitted parameter which represents the sensitivity of stomata to changes in D_s. In this study, all models were applied at the canopy scale. Therefore, the vapor pressure deficit measured near the leaf surface (D_s) was replaced by the one measured in the free air stream (VPD).

2.3.4 The Friend model

Stomatal response to increasing atmospheric demand is accompanied by a linear decline in C_i/C_a (Leuning, 1995). For use in a GCM, Friend and Kiang (2005) parameterized the response of stomatal conductance to specific humidity deficit $\Delta = (q_{sat} - q)$ such that C_i/C_a declined approximately linearly over a normal range of field Δ values, and proposed the following function:

$$f_\Delta = 2.8 \exp(-80\Delta) \tag{11}$$

where f_Δ is relative canopy conductance. In this study, Eq. 11 was incorporated into the equation of the Ball-Berry model. Thus, the final model as tested and evaluated in this study is given by the following equation:

$$g_s = g_0 + g_1 \frac{A_n \, 2.8 \exp(-80\Delta)}{C_a} \tag{12}$$

2.3.5 The unified stomatal model

This approach developed by Medlyn et al. (2011) is a combination of the optimal stomatal conductance model by Cowan and Farquhar (1977) and the photosynthesis model from Farquhar et al. (1980). The combination of the optimal stomatal control model with the equation describing photosynthetic rate limited by RuBP regeneration (Eq. 3) gives the following approximation for the optimal stomatal conductance, hereinafter called the unified stomatal model (USM):

$$g_s \approx g_0 + \left(1 + \frac{g_1}{\sqrt{D_s}}\right) \frac{A_n}{C_a} \tag{13}$$

As claimed by Medlyn et al. (2011), this expression is closely analogous to the empirical models described in sections 2.3.2 and 2.3.3, with the difference that the slope parameter g_1 has now a theoretical underpinning. It was shown that g_1 can be brought into relation with Γ^* and λ in the following way:

$$g_1 \propto \sqrt{\Gamma^* \lambda} \tag{14}$$

where λ is the marginal water cost of plant carbon uptake.

2.3.6 Model parameterization and calculation methods

Under well watered conditions, the slope parameter g_1 is assumed to be constant, but it is likely to vary with environmental conditions or vegetation properties (section 4.3). Since no sufficient infor-

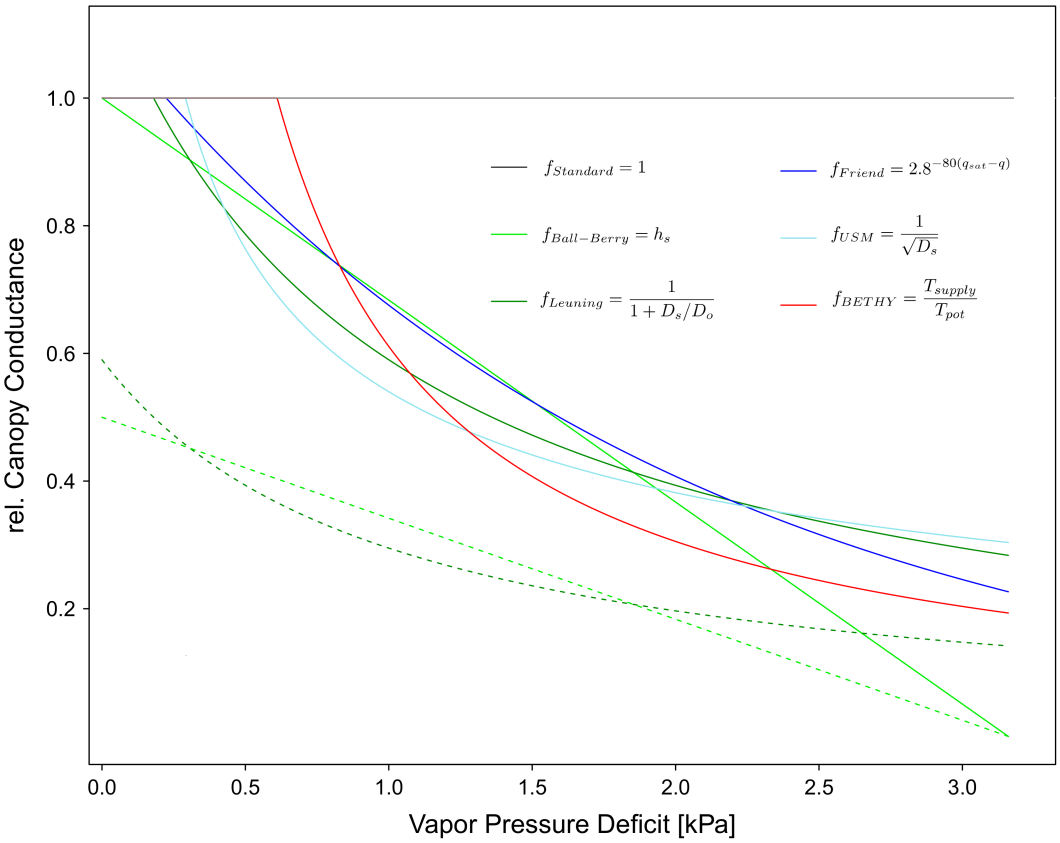

Fig. 2. Functions describing the response of G_c to an increase in VPD for the models evaluated in this study. Relative humidity h_s in the Ball-Berry model and specific humidity q in the Friend model were converted to VPD for a temperature of 25°C. All functions are bounded between 0 and 1. Functions were multiplied by their specific slope relative to the Ball-Berry slope (Leuning: 1.18, Friend: 1.12, USM: 0.54) to allow better comparability. The dashed lines illustrate the effect of soil water stress ($\beta = 0.5$) on the functions applied to the Ball-Berry and Leuning model. The BETHY function shown is based on a T_{max} of 3 mmol m^{-2} s^{-1} and an infinite G_a. Note that the simulated value for stomatal conductance in the models also depends on C_a and A_n and changes with the parameters g_0 and g_1.

mation is available on how this and other parameters vary with plant functional types regionally, parameters are treated as global constants. g_1 in the Ball-Berry model is set to 9.3 for C3 plants as determined by Ball et al. (1987) and to 3.0 for C4 plants according to Collatz et al. (1992). For the other models, g_1 was changed in a way that a similar slope was obtained when plotting g_s against the stomatal response function of the USM (Eq. 13) at a relative humidity range of 40-80%. The values of g_1 used here are: Leuning: 11.0, Friend: 10.4, USM: 5.0. Consequently, the models have similar C_i/C_a responses to increasing VPD. In all models, g_1 responds only to water stress according to Eq. 15. The VPD-sensitivity parameter D_0 in the Leuning model is set to 1 kPa according to estimates for various data sets by Leuning (1995). The residual conductance parameter g_0 is set to 0.01 mol m^{-2} s^{-1} for C3 plants according to Leuning (1990) and to 0.08 mol m^{-2} s^{-1} for C4 plants according to Collatz et al. (1992). The source of the T_{max} parameter in the BETHY-model is described in section 2.3.1. In contrast to the standard model, no potential rates are calculated. Instead, C_i, A_n, and g_s are solved iteratively. A_n is calculated from the Farquhar photosynthesis

scheme (Eq. 1), g_s from the respective stomatal conductance model (Eqs. 9,10,12,13), and C_i is obtained by solving the diffusion equation (Eq. 4). This procedure worked well under well-watered conditions, but became numerically unstable under conditions of soil water stress.

2.4 Representation of soil water stress

Except for the BETHY model, all models considered in this study are developed for conditions of unlimited water supply. The response of stomata to soil water stress is therefore usually accounted for by adding a water stress term to the functions. In this study, this was achieved by applying the following normalized soil moisture dependent function to stomatal conductance:

$$\beta = \begin{cases} 1 & \Theta \geq \Theta_{crit} \\ \frac{\Theta - \Theta_{wilt}}{\Theta_{crit} - \Theta_{wilt}} & \Theta_{wilt} < \Theta < \Theta_{crit} \\ 0 & \Theta \leq \Theta_{wilt} \end{cases} \tag{15}$$

where Θ is volumetric soil water content, Θ_{crit} is the critical soil moisture content, above which plants are considered to be unaffected by water stress, and Θ_{wilt} represents the permanent wilting point, below which water stress is at its maximum. At a soil moisture content between Θ_{crit} and Θ_{wilt}, β declines linearly with declining soil moisture. The function ranges from 0 to 1, with 0 representing maximum soil moisture stress. The final stomatal conductance is then given by:

$$g_s = \beta \cdot f_{g_s} \tag{16}$$

where f_{g_s} stands for the respective stomatal model formulation considered (Eqs. 9,10,12,13). It is worth to mention that Eq. 16 is equivalent to a reduction of the slope parameter g_1 by the factor β.

2.5 JSBACH model runs

JSBACH (Version 2.0) was run at site level for all 58 sites and forced with meteorological measurements from the flux towers. The vegetation in the immediate environment of the tower was assigned to one or several of the PFT-types implemented in JSBACH (Tab. 1). Since not all FLUXNET sites have a homogeneous vegetation cover, two new classes were formed: Temperate open woodland with C3 grass (TeS = TeBEF + TeH) and Savanna with C4 grass (TrS = TrDF + TrH). The assignment was based on land cover information derived from the MODIS land cover product (MCD12Q1), which is mapped using the IGBP land cover classification system (Friedl et al., 2010), and on the climate zone according to the Koeppen-Geiger climate classification. If necessary, the PFT assignment was corrected according to site-specific information from the literature. The modeled maximum LAI and vegetation height were adjusted to the observed values as reported in the FLUXNET ancillary database. Photosynthetic capacity was adjusted to site conditions using light response curves of GPP under favorable atmospheric conditions for photosynthesis and in the absence of soil water stress (Appendix C). Default values as well as adjusted parameter values for all sites can be found in Tab. 2. In most cases, both photosynthetic capacity and LAI were lowered for the site-level runs compared to the default values.

Global JSBACH simulations were conducted for the 30-year time period 1979-2008 for each model version at TM3vfg spatial resolution (approx. 1.875°). The model was not coupled to the MPI-ESM atmosphere component ECHAM6 but forced with the global atmospheric reanalysis ERA-Interim

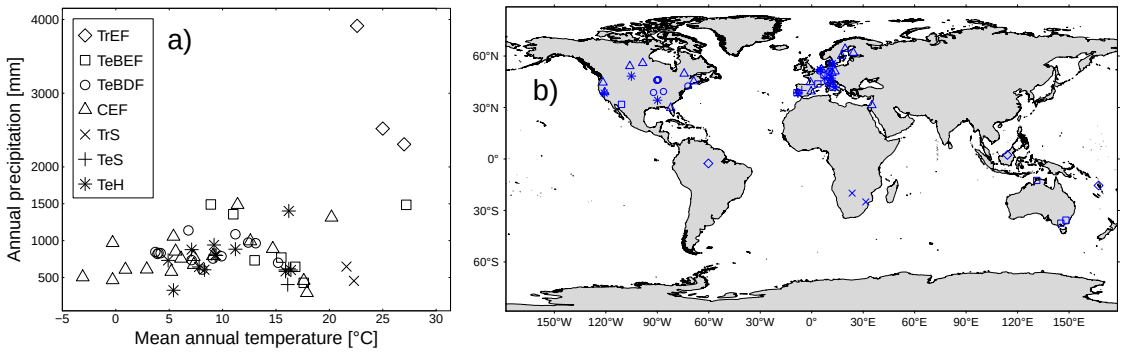

Fig. 3. Distribution of flux tower sites considered in this study (a) in the temperature-precipitation space and (b) geographically. Symbols represent PFTs (TrEF=Tropical evergreen forest, TeBEF=Temperate broadleaf evergreen forest, TeBDF=Temperate broadleaf deciduous forest, CEF=Coniferous evergreen forest, TrS=Savanna with C4 grass, TeS=Temperate open woodland with C3 grass, TeH=C3 grassland).

produced by the ECMWF (Dee et al., 2011). ERA-Interim provides a wide variety of gridded data products, of which atmospheric CO_2, precipitation, specific humidity, wind speed, air temperature, shortwave and longwave radiation were used at daily resolution to force the model. PFT-specific vegetation properties were set to the default values as shown in Tab. 1.

2.6 Eddy covariance flux data

2.6.1 Eddy covariance measurements

Model results at site level were evaluated against carbon and water flux measurements from the FLUXNET network (Baldocchi et al., 2001). FLUXNET is a worldwide network of micrometeorological flux measurement sites that measure the exchange of carbon dioxide, water vapor, and energy between the land surface and the atmosphere on a continuous and long-term basis (Baldocchi et al., 2001). Measurements are based on the eddy covariance method, which is a direct micrometeorological measurement technique for turbulent mass and energy fluxes. It is based on high frequency (10 - 20 Hz) measurements of wind speed and direction using three-dimensional sonic anemometors as well as CO_2 and H_2O concentrations using infrared gas analyzers. The mean covariance between vertical wind velocity and the respective scalar fluctuation is proportional to the flux density. These measurements are usually integrated over periods of half an hour and thus form the basis to calculate fluxes of daily to annual timescales (Baldocchi et al., 2001). Measurements based on the eddy covariance technique represent exchange processes at the ecosystem scale. The flux source area or footprint of a single site typically has longitudinal length scales of several hundred meters (e.g. Rebmann et al., 2005).

2.6.2 Flux data processing

Eddy covariance measurements are subject to missing or unreliable data due to instrument failure or bias or unfavorable micrometeorological conditions which make data gap filling necessary before use (Papale, 2012). Bad quality flux data were gap-filled according to the methodology described in Reichstein et al. (2005), where both the covariation of fluxes with meteorological variables as well as their temporal autocorrelation is taken into account. Daily averages were only used if at least 80% of the respective half-hourly data were original or gap-filled with high confidence according to

Reichstein et al. (2005). Further preprocessing included the correction of the storage component of the carbon flux and the removal of spikes in the half-hourly data as documented by Papale et al. (2006). Since conditions of low atmospheric turbulence can lead to non-negligible advective CO_2 fluxes not detected by the sensor, periods of low turbulent mixing were discarded and gap-filled based on a site-specific friction velocity (u_*) threshold according to Papale et al. (2006).

GPP is not directly measured by the eddy-covariance technique, but derived from net ecosystem exchange (NEE) measurements via a flux partitioning algorithm, which serves to separate NEE into its two components GPP and ecosystem respiration (R_{eco}). In this study, GPP is derived from NEE using the method described by Reichstein et al. (2005), where nighttime ecosystem respiration is extrapolated to daytime using a temperature response function which takes the short-term temperature sensitivity of R_{eco} into account. After the determination of R_{eco}, GPP was calculated as the difference between NEE and R_{eco} (Reichstein et al., 2005).
ET was inferred from the measured latent heat flux. For the separation of transpirational (i.e. physiologically controlled) from non-transpirational water fluxes, days with rainfall and the two subsequent days were excluded if precipitation exceeded 0.2 mm (day with rainfall), 0.5 mm (day before), or 1 mm (two days before). For the remaining days, transpiration was calculated as the average of ET values at daytime, under the assumption that interception storage is largely depleted two days after rain events (Grelle et al., 1997) and soil evaporation is either negligible on sites with a closed canopy or a minor constituent of the total water flux after two dry days (Choudhury and Monteith, 1988). To distinguish between water-stressed and non-water-stressed conditions and therefore separate atmospheric effects on plant physiology from those of soil moisture, site-specific soil moisture thresholds were determined based on derived GPP data (Appendix D.2). All data exceeding the threshold were considered unstressed with regard to water availability.
WUE in this study was calculated as the ratio of daily averages of GPP and ET. Only days within the growing season and time periods when interception and soil evaporation were regarded negligible were considered. Further filtering steps were applied to remove days when mean daily LE < 20 Wm^{-2}, global radiation < 150 Wm^{-2}, and mean air temperature < 0°C, following Kuglitsch et al. (2008). Inherent water use efficiency (IWUE) was calculated as $\frac{GPP \cdot VPD}{ET}$, where VPD represents mean daylight VPD in this case (Beer et al., 2009).
Aerodynamic conductance G_a was calculated as demonstrated in Appendix E. If G_a is known, the canopy conductance G_c can be derived from the inversion of the Penman-Monteith equation (Monteith, 1965):

$$G_c = \frac{\gamma \lambda_w ET\, G_a}{\epsilon R_n + \rho C_p\, VPD\, G_a - \lambda_w(\epsilon + \gamma) ET} \tag{17}$$

where γ is the psychrometric constant, λ_w is the latent heat of vaporization, ϵ is the change of latent heat content relative to the change of sensible heat content of saturated air, R_n is net radiation, and C_p is the specific heat of air. The soil heat flux was neglected. The unit for ET in this case is mol m^{-2} s^{-1}. Throughout the analysis, only data within the growing season were used. Growing season was delineated based on smoothed time series of GPP as described in Appendix D.1. Particularly grassland sites were subject to anthropogenically induced disturbances such as mowing or grazing, which are not accounted for in the model runs. Thus, time periods obviously affected by mowing events were removed. The effect of grazing was accounted for by adjusting LAI to the observed values.
A tabular description of the 58 sites used in this study can be found in Tab. 2. The sites are

distributed around the globe covering a wide range of climatic conditions and biomes (Fig. 3).

2.7 Model evaluation

Analyses were focused on the evaluation of multi-year and multi-site JSBACH runs with eddy covariance data. Flux data were processed and filtered as described in section 2.6.2, and sites were assigned to PFT-classes as shown in Tab. 2. PFT-classes and their major attributes are summarized in Tab. 1. For each FLUXNET site, half-hourly model outputs of G_c, ET, and GPP at daylight within the growing season and under periods of absent to weak soil water stress were split into VPD groups. For each VPD bin, medians of the variables were calculated, provided a sufficient number of data points in the respective bin. Data were then aggregated into PFT-groups and medians and standard errors were calculated based on medians of all sites of the same PFT. The results are shown in Fig. 5-7. Since days with rainfall and preceding days were removed (section 2.6.2), ET was assumed to be dominated by transpiration. Two statistical measures were used to evaluate model performance at site level: the normalized root mean square error (NRMSE) and percent bias (PBIAS). The NRMSE is here calculated as the root mean square error normalized by the mean of the observations (Janssen and Heuberger, 1995):

$$\mathrm{NRMSE} = \frac{\sqrt{\frac{1}{N} \cdot \sum_{i=1}^{N} (Sim_i - Obs_i)^2}}{\overline{Obs}} \tag{18}$$

where Obs are measured or derived flux data, Sim are simulated values, and $\overline{Obs}$ denotes the mean of all flux data. PBIAS is given by:

$$\mathrm{PBIAS} = \frac{\sum_{i=1}^{N} (Sim_i - Obs_i)}{\sum_{i=1}^{N} Obs_i} \cdot 100 \tag{19}$$

Both measures were calculated based on the medians of the VPD-binned data for the whole VPD range (bin width = 0.1 kPa). The NRMSE values were compared using a one-way ANOVA and a Tukey HSD post-hoc analysis for homoscedastic data. In case of a heteroscedastic data distribution within groups, a Welch-ANOVA and the Games-Howell post-hoc test were applied. Homoscedasticity was tested using the Bartlett-test. ANOVA-tests further assume that data follow a normal distribution, which was tested by the Shapiro-Wilk test. For some groups, this assumption was violated, but since studies have shown that ANOVA is robust against violations of the normality assumption (Schmider et al., 2010), the test was applied for all PFTs. The significance level for all tests applied was $p<0.05$. To evaluate the overall model performance (i.e. under water-stressed and unstressed conditions) for all model versions, NRMSE and PBIAS were calculated for daily ET and GPP values for all sites (Tab. 4). All statistical analyses were conducted in R (Version 3.02) (R Core Team, 2013).

Global model simulations were compared to upscaled FLUXNET observations from Jung et al. (2011), hereinafter named MTE-product. For this product, GPP and latent heat flux were predicted using a machine learning method ("model tree ensembles" (MTE)) based on remote sensing indices, climate and meteorological data, and land use information. The generated flux fields span the time period from 1982 to 2008 at monthly resolution. Global means of annual GPP were compared to the results of Beer et al. (2010), who provide a observation-based estimate of annual

GPP based on eddy covariance data and diagnostic models. Likewise, global annual mean values of ET were compared to the global land ET synthesis product by Müller et al. (2013), which is based on various global diagnostic data sets of ET as well as on results from LSMs for the time period 1989-2005.

Carbon uptake was highly overestimated in arid regions, probably due to a missing process component in the plant drought response (section 4.4). Therefore, regions with less than 150 mm precipitation per year were masked out in the global maps, but considered for the latitudinal plots and the calculation of global mean values.

Tab. 2. Characteristics of flux tower sites used in this study

	Site[a]	Lat	Long	Climate[b]	PFT[c]	default LAI[d]	default Vcmax[e]	adjusted LAI[d]	adjusted Vcmax[e]	Reference
1	AT-Neu	47.12	11.32	Cfb	TeH	2.3	78.2	6.5	39.6	Wohlfahrt et al. (2008b)
2	AU-How	-12.49	131.15	Aw	TeBEF	4.0	45.7	2.4	27.0	Beringer et al. (2011)
3	AU-Tum	-35.66	148.15	Cfb	TeBEF	5.5	62.2	2.4	51.3	Cleugh et al. (2007)
4	AU-Wac	-37.43	145.19	Cfb	TeBEF	5.5	62.2	5.5	43.2	Martin et al. (2007)
5	BE-Bra	51.31	4.52	Cfb	TeBDF	4.5	61.0	2.8	38.1	Carrara et al. (2004)
6	BR-Ma2	-2.61	-60.21	Af	TrEF	6.8	39.0	5.2	41.6	Araújo et al. (2002)
7	BW-Ma1	-19.92	23.56	BSh	TrS	5.9	30.8	1.3	245.6	Veenendaal et al. (2004)
8	CA-Man	55.88	-98.48	Dfc	CEF	4.4	64.1	4.2	26.0	Dunn et al. (2007)
9	CA-Qfo	49.69	-74.34	Dfc	CEF	4.4	64.1	3.7	25.4	Bergeron et al. (2007)
10	CA-SF3	54.09	-106.00	Dfc	CEF	4.4	64.1	1.1	40.0	Mkhabela et al. (2009)
11	CH-Oe1	47.29	7.73	Cfb	TeH	2.3	78.2	4.8	41.0	Ammann et al. (2007)
12	DE-Bay	50.14	11.87	Cfb	CEF	4.4	64.1	5.3	34.4	Rebmann et al. (2004)
13	DE-Hai	51.08	10.45	Cfb	TeBDF	4.5	58.7	6.1	44.8	Kutsch et al. (2008)
14	DE-Meh	51.28	10.66	Cfb	TeH	2.3	78.2	2.8	34.6	Scherer-Lorenzen et al. (2007)
15	DE-Tha	50.96	13.57	Cfb	CEF	4.4	64.1	8.0	35.4	Grünwald and Bernhofer (2007)
16	DK-Lva	55.68	12.08	Cfb	TeH	2.3	78.2	6.9	34.7	Gilmanov et al. (2007)
17	DK-Sor	55.49	11.65	Cfb	TeBDF	4.5	58.7	5.0	57.0	Lagergren et al. (2008)
18	ES-ES1	39.35	-0.32	Csa	CEF	4.4	64.1	2.6	33.0	Sanz et al. (2004)
19	ES-LMa	39.94	-5.77	Csa	TeS	3.3	73.2	2.0	44.3	Vargas et al. (2013)
20	FI-Hyy	61.85	24.29	Dfc	CEF	4.4	64.1	6.7	24.8	Suni et al. (2003)
21	FR-Hes	48.67	7.06	Cfb	TeBDF	4.5	58.7	6.7	42.5	Granier et al. (2000)
22	FR-LBr	44.72	-0.77	Cfb	CEF	4.4	64.1	3.5	52.3	Berbigier et al. (2001)
23	FR-Pue	43.74	3.60	Csa	TeBEF	5.5	62.2	2.9	37.7	Keenan et al. (2010)
24	ID-Pag	2.35	114.04	Af	TrEF	6.8	39.0	5.6	32.8	Hirano et al. (2007)
25	IL-Yat	31.34	35.05	BSh	CEF	4.4	64.1	2.5	28.6	Grünzweig et al. (2003)
26	IT-Amp	41.90	13.61	Cfa	TeH	2.3	78.2	2.4	47.3	Wohlfahrt et al. (2008a)
27	IT-Cpz	41.71	12.38	Csa	TeBEF	5.5	62.2	3.5	34.1	Tirone et al. (2003)
28	IT-Lav	45.96	11.28	Cfb	CEF	4.6	61.8	8.1	32.0	Marcolla et al. (2003)
29	IT-MBo	46.02	11.05	Cfb	TeH	2.3	78.2	2.9	43.8	Wohlfahrt et al. (2008a)
30	IT-PT1	45.20	9.06	Cfa	TeBDF	4.5	58.7	2.0	84.6	Migliavacca et al. (2009)
31	IT-Ro2	42.39	11.92	Csa	TeBDF	4.5	58.7	3.9	37.7	Tedeschi et al. (2006)
32	IT-SRo	43.73	10.28	Csa	CEF	4.4	64.1	4.2	31.8	Chiesi et al. (2005)
33	NL-Ca1	51.97	4.93	Cfb	TeH	2.3	78.2	11.3	14.5	Jacobs et al. (2007)
34	NL-Hor	52.03	5.07	Cfb	TeH	2.3	78.2	3.3	24.1	Jacobs et al. (2007)
35	NL-Loo	52.17	5.74	Cfb	CEF	4.4	64.1	2.0	64.5	Dolman et al. (2002)
36	PT-Esp	38.64	-8.60	Csa	TeBEF	5.5	62.2	2.8	45.6	Pereira et al. (2007)
37	PT-Mi1	38.54	-8.00	Csa	TeS	4.0	69.8	0.7	262.9	Pereira et al. (2007)
38	PT-Mi2	38.48	-8.02	Csa	TeH	2.3	78.2	1.6	34.4	Pereira et al. (2007)
39	SE-Fla	64.11	19.46	Dfc	CEF	4.4	64.1	3.4	27.0	Lindroth et al. (2008)
40	SE-Nor	60.09	17.48	Dfb	CEF	4.4	64.1	4.8	43.8	Lagergren et al. (2008)
41	US-Blo	38.90	-120.63	Csa	CEF	4.4	64.1	4.6	25.0	Goldstein et al. (2000)
42	US-FPe	48.31	-105.10	BSk	TeH	2.3	73.4	2.5	12.5	Wilson and Meyers (2007)
43	US-Goo	34.25	-89.87	Cfa	TeH	2.3	58.9	2.0	48.4	Wilson and Meyers (2007)
44	US-Ha1	42.54	-72.17	Dfb	TeBDF	4.5	58.7	5.4	38.4	Urbanski et al. (2007)
45	US-Ho1	45.20	-68.74	Dfb	CEF	4.4	64.1	6.5	33.5	Hollinger et al. (1999)
46	US-Los	46.08	-89.98	Dfb	TeBDF	4.5	58.7	4.2	26.7	Sulman et al. (2009)
47	US-Me4	44.50	-121.62	Csb	CEF	4.4	64.1	2.1	30.4	Law et al. (2001)
48	US-MMS	39.32	-86.41	Cfa	TeBDF	4.5	58.7	4.8	31.5	Schmid et al. (2000)
49	US-MOz	38.74	-92.20	Cfa	TeBDF	4.5	58.7	4.2	39.0	Gu et al. (2006)
50	US-PFa	45.95	-90.27	Dfb	TeBDF	4.5	60.0	4.4	33.4	Davis et al. (2003)
51	US-SP3	29.75	-82.16	Cfa	CEF	4.4	64.1	6.4	23.7	Clark et al. (1999)
52	US-SRM	31.82	-110.87	BSk	TrS	4.0	45.7	0.5	79.2	Scott et al. (2009)
53	US-Syv	46.24	-89.35	Dfb	TeBDF	4.5	61.0	7.5	28.2	Desai et al. (2005)
54	US-Ton	38.43	-120.97	Csa	TeS	3.7	65.9	1.3	69.7	Ma et al. (2007)
55	US-Var	38.41	-120.95	Csa	TeH	2.3	78.2	2.4	40.9	Ma et al. (2007)
56	US-WCr	45.81	-90.08	Dfb	TeBDF	4.5	58.7	5.4	45.4	Cook et al. (2004)
57	VU-Coc	-15.44	167.19	Af	TrEF	6.8	39.0	5.7	40.4	Roupsard et al. (2006)
58	ZA-Kru	-25.02	31.50	Cwa	TrS	3.7	30.3	1.7	29.1	Archibald et al. (2010)

[a] Station IDs consist of two characters describing the country and three characters as abbreviation for the site name (cf. http://www.fluxnet.ornl.gov/site_status).

[b] Koeppen-Geiger climate zone (Af = equatorial, rainforest; Aw = equatorial, monsoonal; BSh = hot arid steppe; BSk = cold arid steppe; Cfa = humid, warm temperate, hot summer; Cfb = humid, warm temperate, warm summer; Csa = summer dry, warm temperate, hot summer; Csb = summer dry, warm temperate, warm summer; Cwa = winter dry, warm temperate, hot summer; Dfb = Cold, humid, warm summer; Dfc = Cold, humid, cold summer).

[c] Plant functional type (TrEF = Tropical evergreen forest, TeBEF = Temperate broadleaf evergreen forest, TeBDF = Temperate broadleaf deciduous forest, CEF = Coniferous evergreen forest, TrS = Savanna with C4 grass, TeS = Temperate open woodland with C3 grass, TeH = C3 grassland).

[d] maximum LAI in the growing season.

[e] at the reference temperature of 25°C.

3 Results

3.1 Mean daily courses

Mean diurnal courses of three sunny days without water stress for a temperate deciduous forest are shown in Fig. 4. For all models, G_c is considerably reduced throughout the day compared to the standard version, and is therefore closer to the values as inverted from the Penman-Monteith equation. The response of stomata to atmospheric drought becomes apparent as G_c decreases during the day along with an increase in VPD. Differences between the alternative model versions reflect the different sensitivities to atmospheric humidity (Fig. 2). In general, differences between the models are relatively low compared to the standard version, only the BETHY model shows a different behavior such as higher G_c in the morning and lower G_c in the afternoon. The reduced G_c leads to lower ET rates. As ET depends on VPD, clear differences between the models only occur at times when VPD is high. Since the model versions are based on the close correlation between GPP and G_c, both variables show a similar behavior throughout the day, with the largest decrease in the evening, at times when VPD is highest. This leads to a better model performance, both qualitatively and quantitatively.

3.2 Model performance with respect to atmospheric dryness

Model performance of G_c split into classes of VPD (bin width = 0.4 kPa) is shown in Fig. 5. Model performance is expressed as relative bias (i.e. relative deviation) to the derived flux data. Compared to the standard model, which highly overestimates G_c particularly under conditions of high VPD, the alternative models give better results and are in general close to the derived values from the flux data. Differences between models are not clearly recognizable. An exception is the BETHY model, which overestimates G_c for savanna-like ecosystems and grasslands, resulting in only slight improvements for these ecosystems. The changes in G_c are reflected in ET (Fig. 6), which is persistently too high in the standard model under dry atmospheric conditions and is significantly lower in the alternative models. However, the alternative models reduce ET less strongly than G_c. Again only minor differences between the model versions can be observed, except for the BETHY model, which overestimates ET for grasslands and savanna-like ecosystems. Under conditions of low VPD, all model versions underestimate ET. GPP (Fig. 7) is affected by a decline in G_c similarly to ET. All models show similar deviations under low VPD as photosynthetic capacity was adjusted to site conditions (Appendix C). Despite this adjustment, simulated GPP in the standard model is overestimated under conditions of high VPD, except for savannas (Fig. 5). The alternative models show again lower deviations compared to the standard model, but generally overestimate GPP for grasslands.

Calculated NRMSEs for all PFTs are shown in Fig. 8. For G_c, differences between the standard model and the alternative models based on a photosynthesis-stomatal conductance scheme (Ball-Berry, Leuning, Friend, USM) are statistically significant for all forest ecosystems but not for savanna-like sites and grasslands. For the savanna-like ecosystems, this may be due to the low sample size (n=3). Regardless of statistical significance, all model variants show considerable improvements. One exception is again the BETHY model for ecosystems with a high fraction of grasslands. The reason for this might be the parameterization of the model (section 4.1). Apart from that, no significant differences occur between the alternative models. Same holds true for ET,

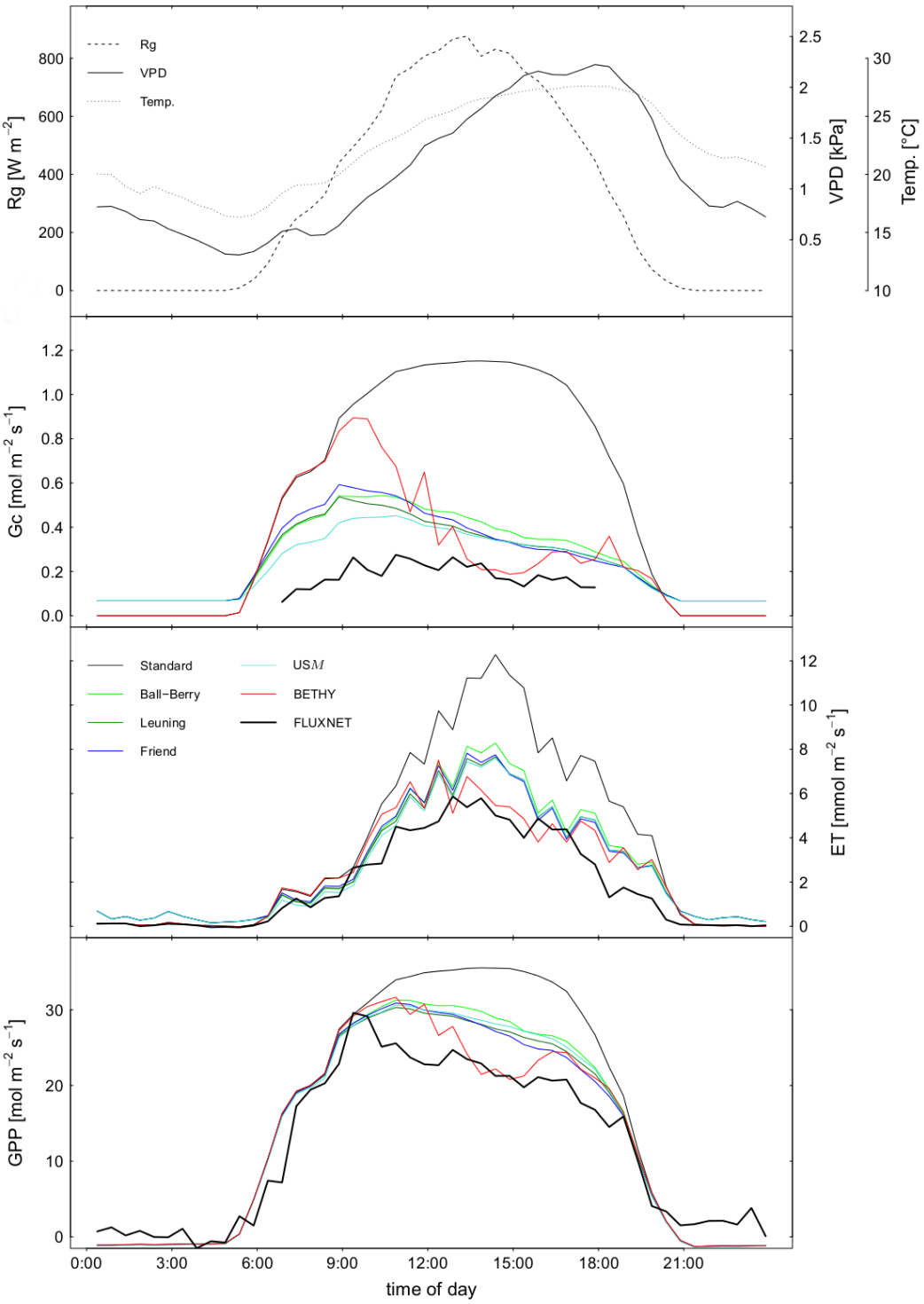

Fig. 4. Mean diurnal course (1st - 3rd July 2005) of meteorological variables and G_c, ET, and GPP for the different model versions for a broadleaf deciduous forest (station FR-Hes) in the absence of water stress. No rainfall occurred on the two preceding days, therefore ET is assumed to be dominated by transpiration.

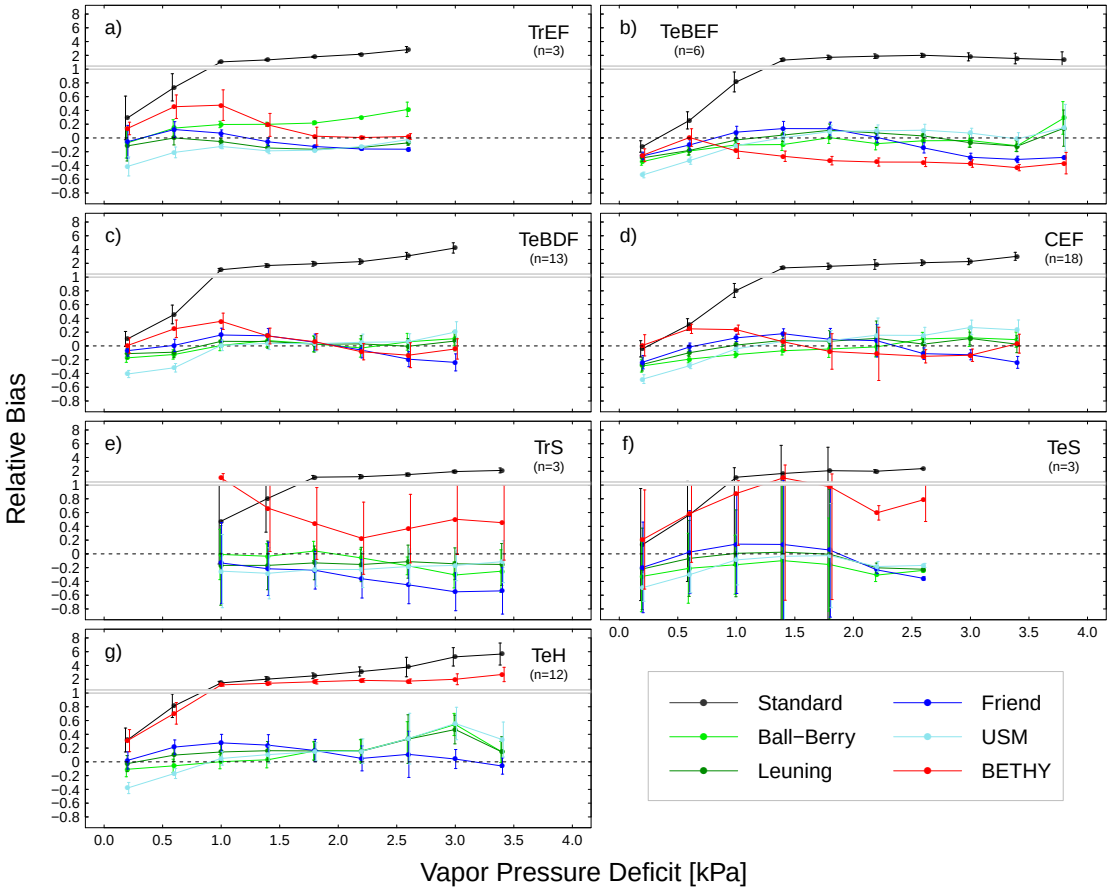

Fig. 5. Relative deviation between the different models and the derived flux data (dashed line) for G_c. Values represent PFT-medians based on half-hourly model outputs of G_c under optimal conditions (values are based on half-hourly data at daylight, within the growing season and in the absence of soil water stress). Error bars represent standard errors of the median. PFT-abbreviations: TrEF = tropical evergreen forest, TeBEF = temperate broadleaf evergreen forest, TeBDF = temperate broadleaf deciduous forest, CEF = coniferous evergreen forest, TrS = Savanna with C4 grass, TeS = Temperate open woodland with C3 grass, TeH = C3 grassland.

where the inclusion of the stomatal response to atmospheric humidity leads to improved model performance for all PFTs, even though this is not statistically significant in most cases. The clearest effects can be observed for forested ecosystems, while improvements for grasslands and open woodlands are less pronounced and the NRMSE decreases only slightly compared to the standard model in these ecosystems. The situation is similar for GPP, however, no improvements are achieved for savanna sites. This is most likely due to a single site, where GPP is highly underestimated (USSRM), probably due to an erroneous maximum LAI value. Differences in NRMSE between the standard model and the Ball-Berry model ($\mathrm{NRMSE_{Ball\text{-}Berry}}$ - $\mathrm{NRMSE_{Standard}}$) are calculated for all sites and plotted against the mean growing season VPD. The results (Fig. 9) demonstrate that both ET and GPP show improved performance for most of the sites, independent of the local mean growing season VPD. Linear regression yields a weak positive slope, which is due to the very high, and most likely erroneous, VPD values measured at one site. After removing the site from the analysis, no statistically significant slope ($p<0.05$) is observed for neither ET nor GPP.

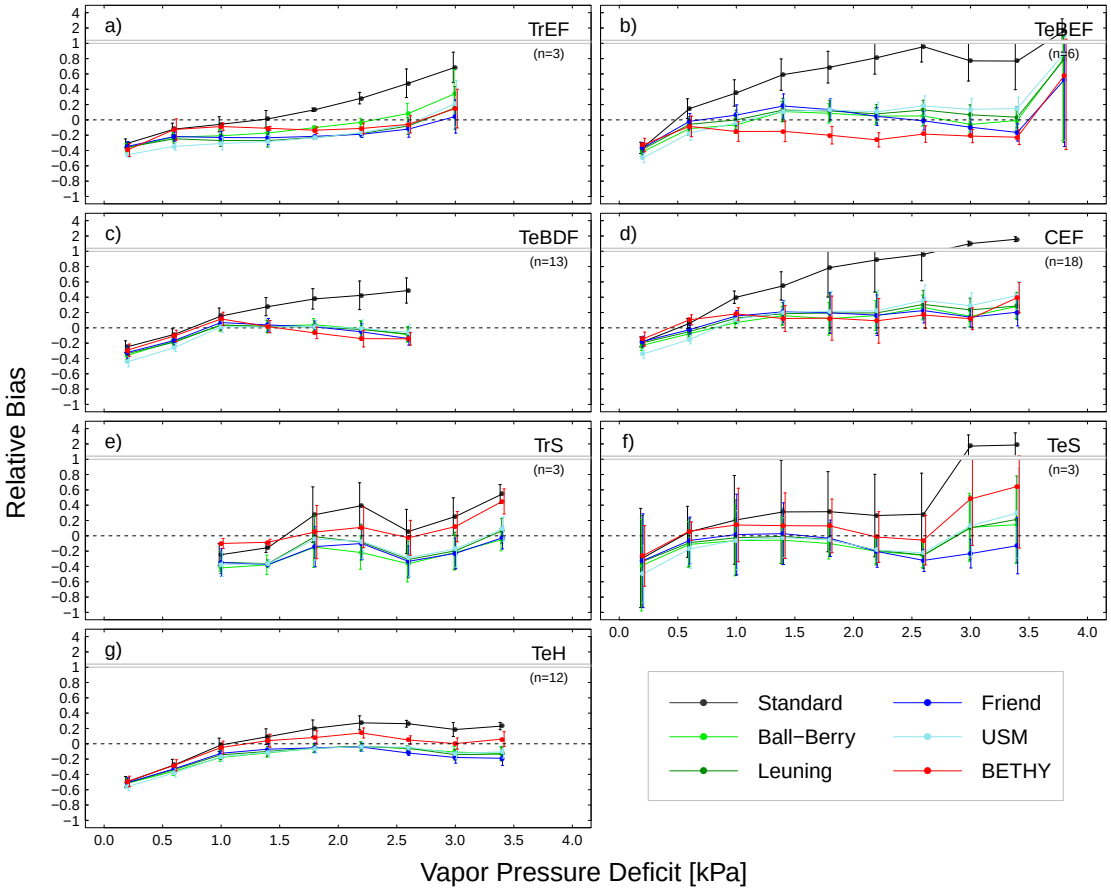

Fig. 6. Relative deviation between the models and the observed flux data (dashed line) for ET. Values represent PFT-medians based on half-hourly model outputs of ET under optimal conditions (values are based on half-hourly data at daylight, within the growing season and in the absence of soil water stress). Error bars represent standard errors of the median. PFT-abbreviations as in Fig. 5.

3.3 Overall model performance

Mean growing season WUE (Fig. 10) is generally overestimated. This is the case for both WUE and IWUE. The latter was calculated to account for the confounding effect of VPD on transpiration and therefore WUE. The standard model WUE is closer to the observed values for almost all PFTs. Differences between PFTs are low, IWUE is mostly in the range of 2-3 gC $kg^{-1}H_2O$ kPa. Savanna-like ecosystems show higher IWUE, the skewed distribution for tropical savannas, however, is due to an outlier and must be interpreted with care. Considerably high or low values occur also in other PFTs, most likely due to bad quality of the VPD-data. Interestingly, WUE and IWUE vary consistently between the models, except for the BETHY scheme. The USM model for instance predicts the highest and the Friend model the lowest IWUE values for almost all PFTs.

Performance measures for the different models are shown in Tab. 4. The statistics were calculated on a daily basis for all time periods, including water stressed conditions. Model performance does not or only slightly improve for tropical rainforests and savannas, but remarkable improvements are made for all other forested ecosystems, especially for ET. Grasslands show slight, but consistent improvements for all models. Differences between models are again low, however, the Ball-Berry approach shows the best results for many PFTs, especially for ET. If all sites are considered,

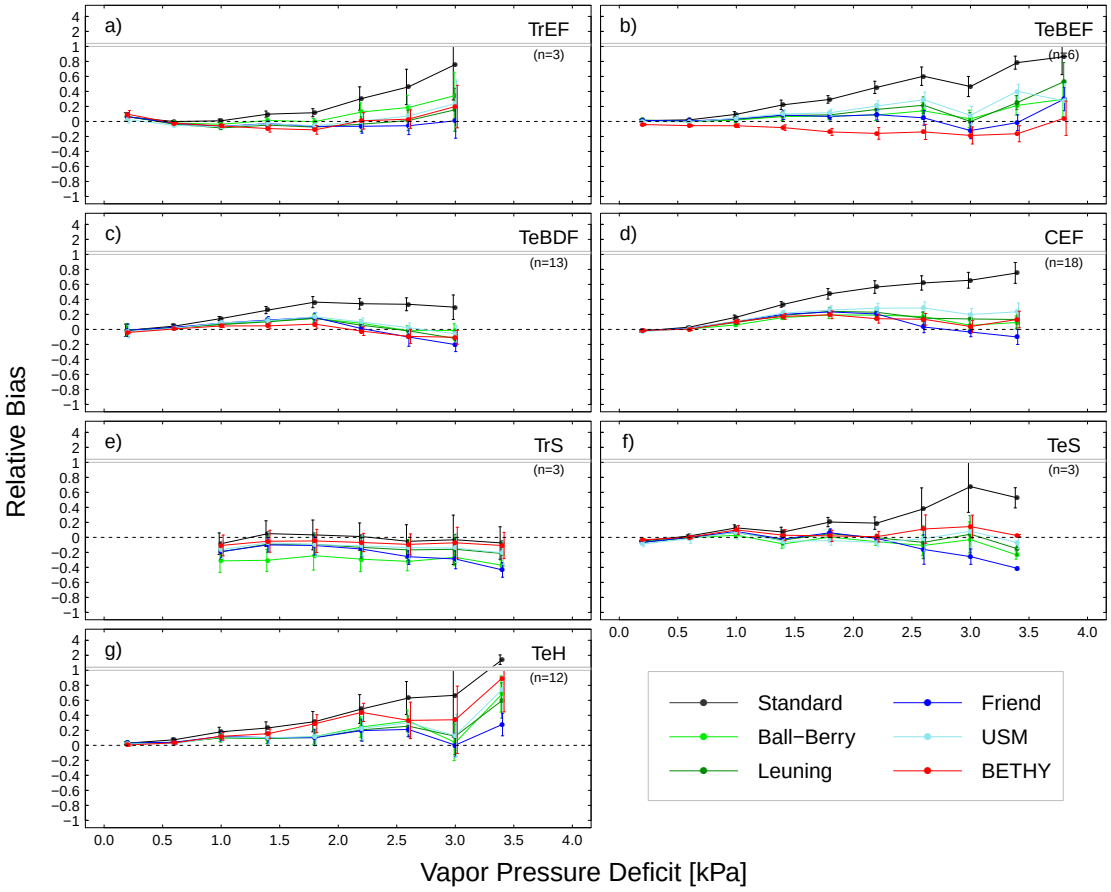

Fig. 7. Relative deviation between the models and the derived flux data (dashed line) for GPP. Values represent PFT-medians based on half-hourly model outputs of GPP under optimal conditions (values are based on half-hourly data at daylight, within the growing season and in the absence of soil water stress). Error bars represent standard errors of the median. PFT-abbreviations as in Fig. 5.

substantial improvements of both NRMSE and PBIAS occur for ET (e.g. NRMSE declines from 0.91 to 0.79 for the Ball-Berry version) and slight improvements for GPP. Since the results include water stressed periods, further improvements can be expected when soil moisture is adequately represented in the model (section 4.4).

3.4 Global simulations

All models show reductions of ET in northern latitudes and in the tropics (Fig. 11b-f). ET remains constant in dry regions such as large parts of Africa and Australia, as well as in Central Asia and Central North America. Large-scale increases occur only over the Tibetan Plateau. The Ball-Berry model shows the largest reductions in boreal regions. In the tropics, the largest decreases occur in simulations with the Friend model. The BETHY model shows much lower decreases in all parts of the world though spatial patterns are similar to the other models. GPP shows a distinct behavior in all models. Large reductions of up to 50% occur in humid regions of the world and large increases in areas characterized by low annual precipitation. The high dependency of GPP on water availability in the global simulations, however, is most likely due to numerical instabilities resulting from an inappropriate process representation of photosynthesis under conditions of water stress. An ecological explanation for the high productivity in context with the stomatal response

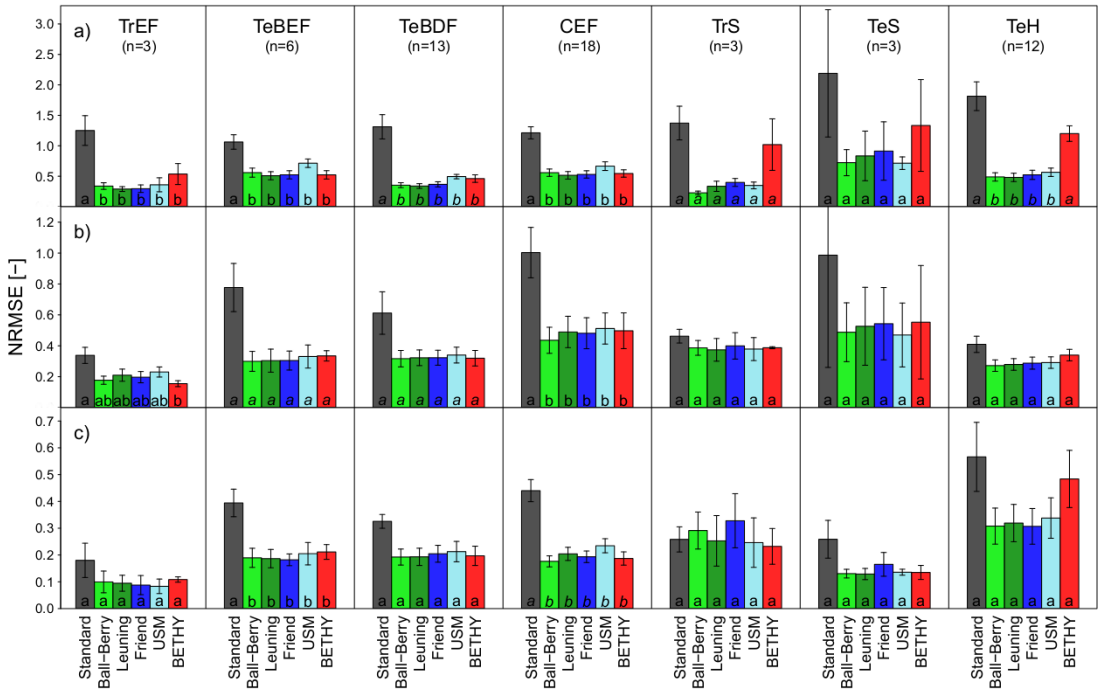

Fig. 8. Normalized root mean square error calculated for (a) G_c, (b) ET, and (c) GPP based on half-hourly model outputs aggregated into bins of VPD (bin width = 0.1 kPa). Shown are PFT-means (± standard errors). Letters indicate differences between means (normal font = Tuckey HSD test, $p<0.05$; *italic* = Games-Howell test, $p<0.05$). PFT-abbreviations as in Fig. 5.

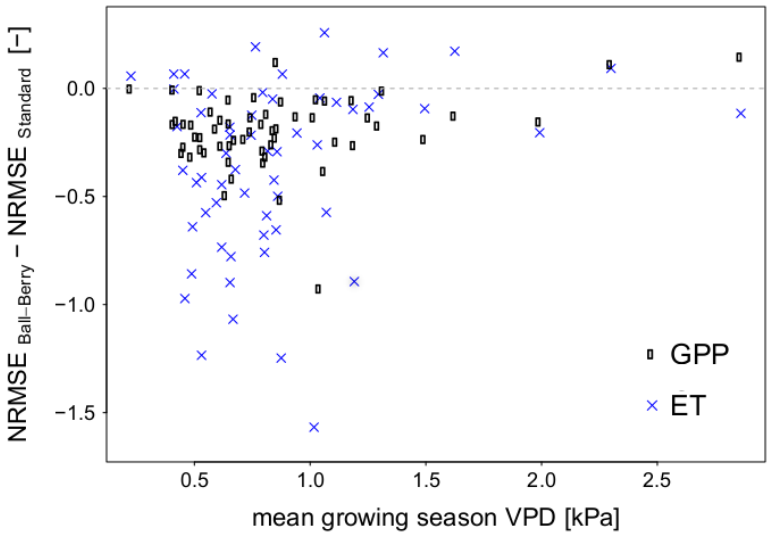

Fig. 9. Difference in normalized root mean square error between the standard and Ball-Berry model for ET and GPP for all sites. Negative values indicate improved model performance compared to the standard version.

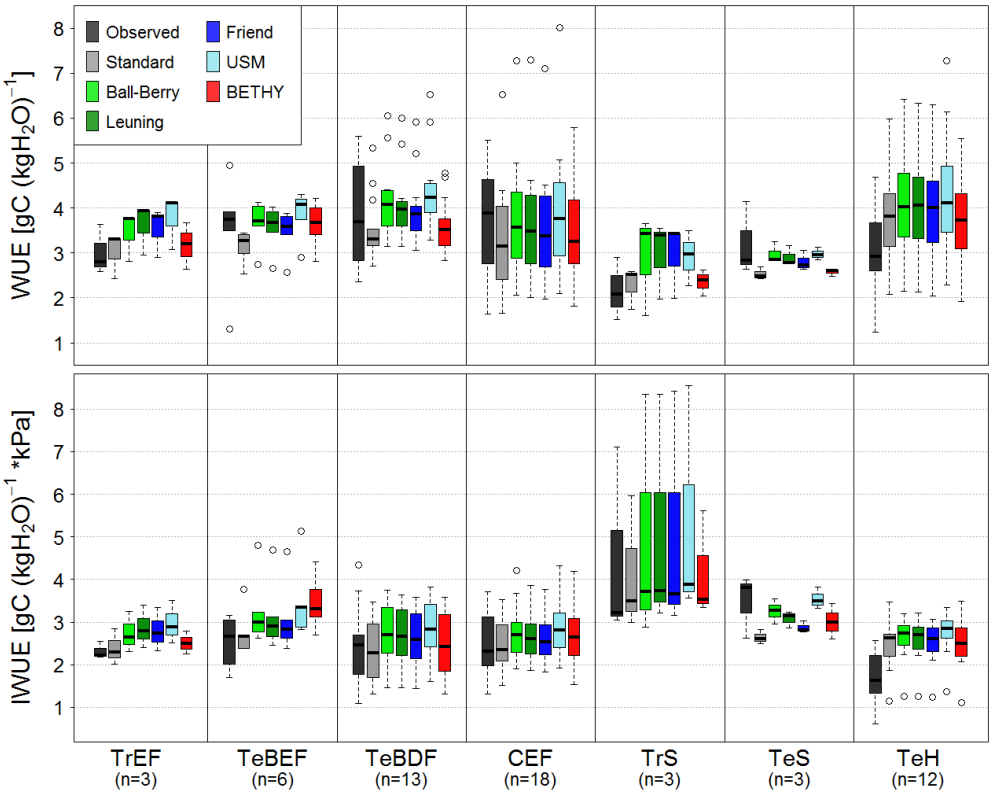

Fig. 10. (upper panel) Mean growing season WUE and (lower panel) mean growing season IWUE as calculated from FLUXNET data for the different model versions and plant functional types. PFT-abbreviations as in Fig. 5.

to VPD does not exist.

The comparison with the MTE-product illustrates the large discrepancies between upscaled flux data and JSBACH model simulations (Ball-Berry version). What catches the eye first is the extreme overestimation of GPP in the Ball-Berry model, despite the large reductions achieved. The new model versions are therefore likely to be an improvement over the standard model. Relative deviations from the MTE-product are comparatively low in the tropics, but high in boreal and arid regions. Results are less uniform for ET, where JSBACH predicts much higher fluxes (up to 100% in boreal regions of North America and Eurasia), but lower values for sub-humid and monsoonal regions in Africa and Asia.

Such differences are emphasized by plots showing latitudinal patterns of ET and GPP (Fig. 13), which reveal remarkable latitudinal differences between the models. ET is consistently lower for all model versions compared to the standard model, whereby the Friend model shows the largest reductions in the tropics and Ball-Berry in latitudes north of 40°. Relative changes are in the order of a few percent, therefore considerable absolute changes occur only in the tropics. The picture is different for GPP, where significant decreases in the tropics stand in contrast to considerable increases in the subtropics, especially in the northern hemisphere. The models show similar patterns but different relative changes in GPP for particular latitudinal bands. The Friend model shows the largest decrease of around 25% in the tropics while the Ball-Berry model reduces GPP by about 15% around the equator. This difference is partly offset by a stronger decrease in the temperate zones of both hemispheres in the Ball-Berry version. The BETHY model again shows a dissimilar

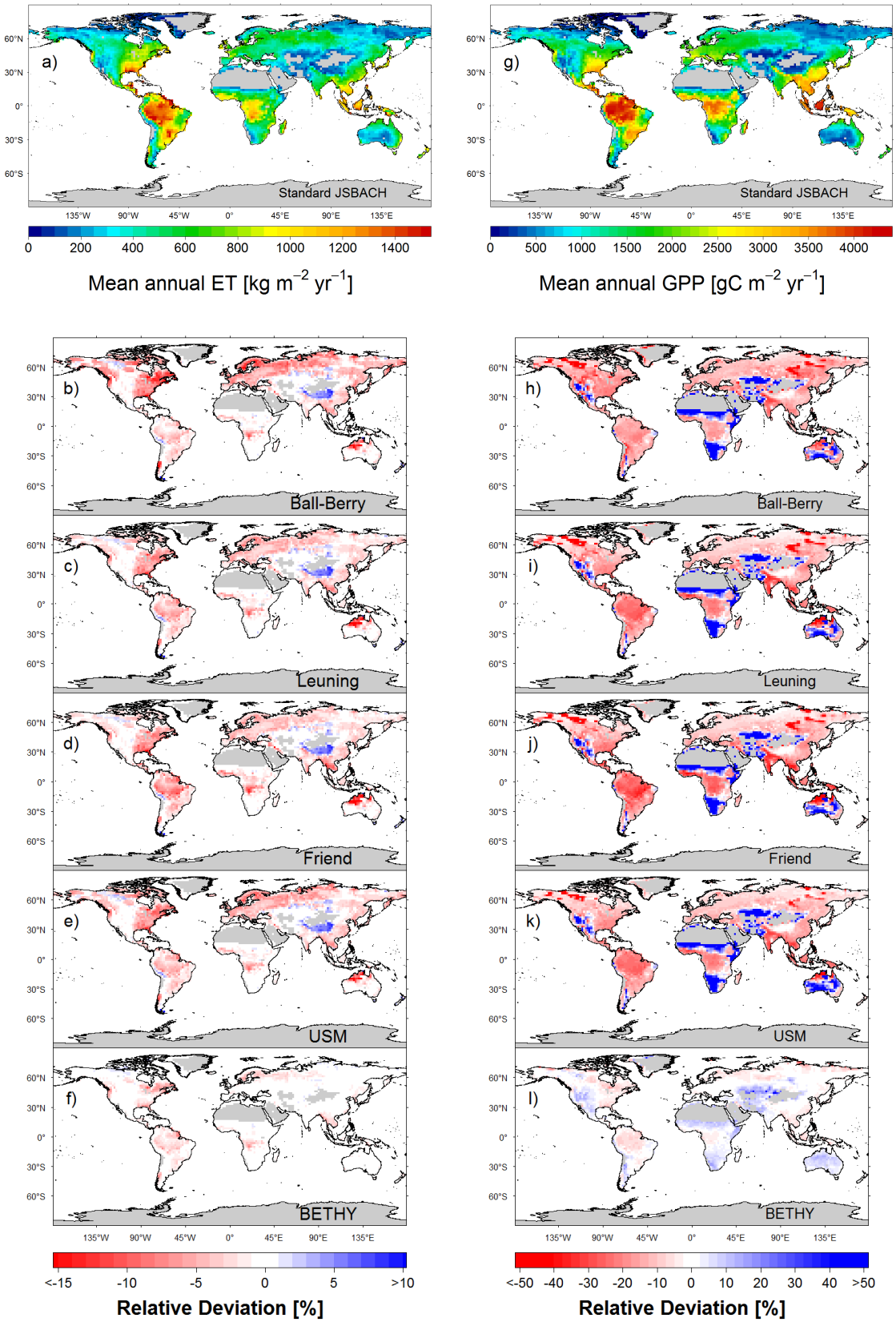

Fig. 11. Mean annual values of (a) ET and (g) GPP of the standard model version and relative deviations of the alternative models from the standard model for (b-e) ET and (h-l) GPP for the time period 1979-2008. Red colors indicate reductions compared to the standard model.

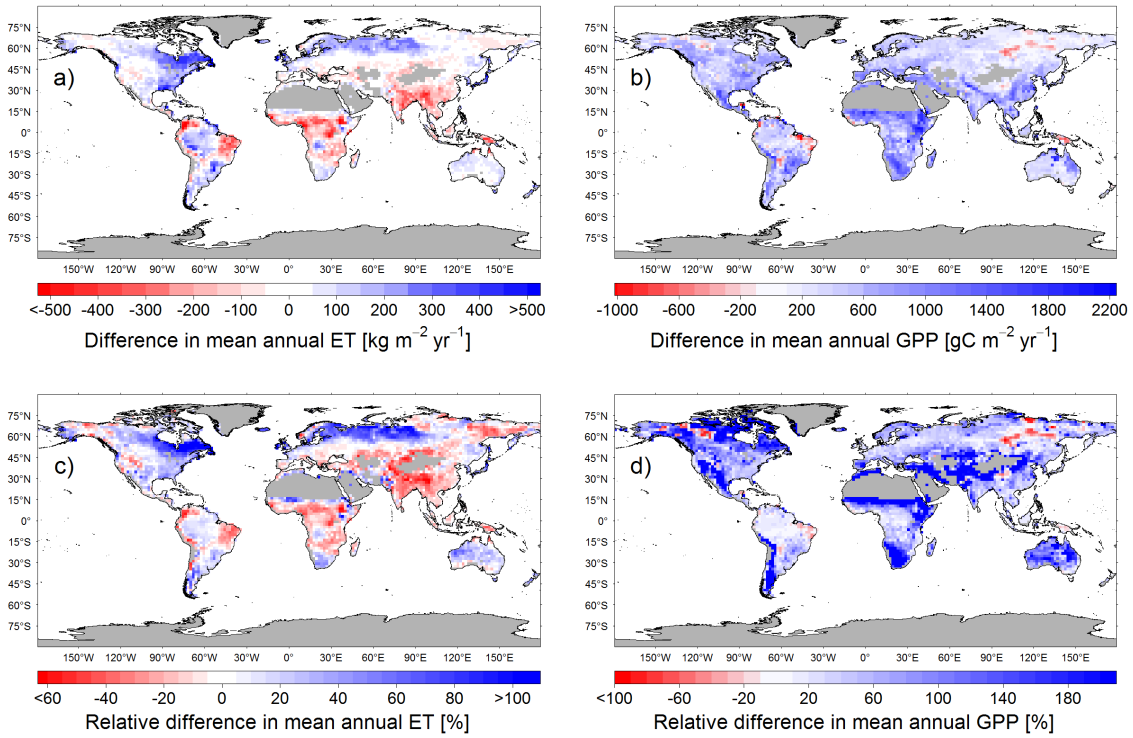

Fig. 12. Absolute and relative differences of (a,c) ET and (b,d) GPP between the Ball-Berry model and the global ET- and GPP-products based on upscaled FLUXNET data by Jung et al. (2011). Red colors indicate lower simulated values compared to the MTE-product.

behavior compared to the other models. Reductions in the tropics and temperate zones are much lower (less than 5%) and no significant overestimation occurs in dry regions. The models evaluated in this study show remarkable absolute decreases of GPP in the tropics, which, to a small extent, are offset by an increase in arid regions of the world. Globally, this leads to a decline in annual GPP by 2 - 18 Gt yr^{-1}. The reduction is mainly a consequence of reduced GPP in the tropics. In comparison to the global means of annual GPP as determined by Beer et al. (2010), JSBACH shows much higher values in all model variants, but the new versions reduce this offset (Tab. 3). Compared to the ET-synthesis product provided by (Müller et al., 2013), global mean annual ET is underestimated by all model versions.

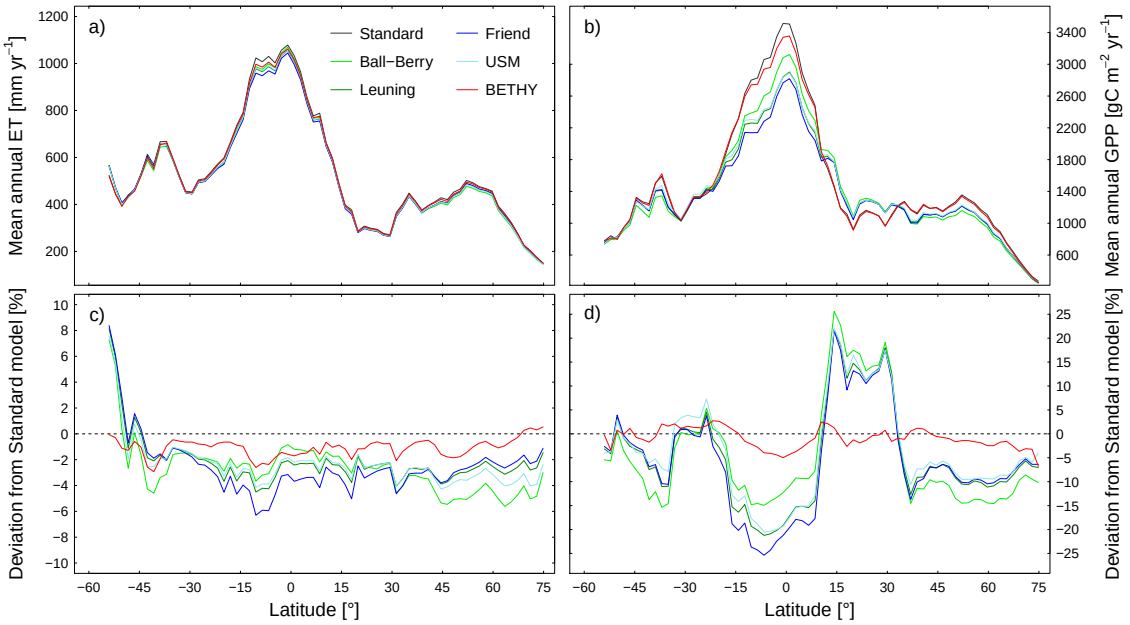

Fig. 13. Latitudinal patterns (1.875° bands) and relative deviations from the standard model shown for zonally averaged annual values of (a,c) ET and (b,d) GPP. Negative values in panels c) and d) indicate lower simulated fluxes compared to the standard model.

Tab. 3. Global mean values of ET and global sums of GPP for the different model versions

	ET [mm yr^{-1}]	GPP [Gt yr^{-1}]
Standard	474	202
Ball-Berry	459	191
Leuning	461	188
Friend	459	184
USM	460	190
BETHY	469	200
Reference	493[a]	123 (8)[b]

[a] Müller et al. (2013)

[b] Beer et al. (2010), standard deviation shown in brackets

Tab. 4. Evaluation measures for all model versions

	Standard		Ball-Berry		Leuning		Friend		USM		BETHY	
	NRMSE	PBIAS [%]	NRMSE	PBIAS [%]	NRMSE	PBIAS [%]	NRMSE	PBIAS [%]	NRMSE	PBIAS [%]	NRMSE	PBIAS [%]
ET:												
TrEF	**0.33 (0.09)**	**-10.05 (8.51)**	0.35 (0.09)	-22.84 (8.74)	0.39 (0.09)	-29.19 (8.86)	0.38 (0.09)	-27.41 (9.04)	0.4 (0.09)	-31 (8.56)	0.35 (0.09)	-23.67 (7.96)
TeBEF	0.79 (0.1)	11.8 (12.65)	**0.61 (0.06)**	**0.19 (11.55)**	0.63 (0.07)	2.29 (11.85)	0.63 (0.07)	3.26 (12.09)	0.62 (0.06)	-0.28 (11.56)	0.62 (0.06)	-4.15 (11.14)
TeBDF	1.11 (0.11)	29.13 (12.44)	**0.97 (0.08)**	14.11 (10.81)	0.99 (0.08)	15.1 (11.02)	1 (0.08)	16.75 (11.14)	0.99 (0.08)	**11.08 (10.74)**	1.01 (0.08)	18.67 (10.83)
CEF	0.99 (0.09)	12.94 (7.3)	**0.81 (0.08)**	0.88 (6.35)	0.84 (0.08)	3.42 (6.65)	0.85 (0.08)	4.56 (6.73)	0.83 (0.08)	**0.7 (6.57)**	0.85 (0.09)	3.15 (6.98)
TrS	1.14 (0.3)	-2.77 (17.5)	**1.1 (0.3)**	-3.27 (17.48)	1.11 (0.3)	-3.19 (17.45)	1.12 (0.29)	-3.27 (17.45)	1.11 (0.3)	-3.15 (17.46)	1.13 (0.31)	**-2.73 (17.49)**
TeS	1.25 (0.65)	40.05 (49.24)	1.03 (0.5)	30.25 (42.57)	1.05 (0.52)	31.25 (42.87)	1.06 (0.52)	31.76 (43.21)	**1 (0.48)**	28.36 (40.33)	1.1 (0.57)	38.13 (47.51)
TeH	0.66 (0.09)	**-1.97 (9.28)**	**0.61 (0.08)**	-9.67 (8.23)	0.62 (0.08)	-8.57 (8.4)	0.62 (0.08)	-7.82 (8.52)	0.63 (0.08)	-10.67 (8.32)	0.64 (0.08)	-3.6 (9.23)
All sites	0.91 (0.06)	12.76 (5.04)	**0.79 (0.05)**	1.67 (4.42)	0.81 (0.05)	2.85 (4.55)	0.81 (0.05)	3.94 (4.6)	0.81 (0.05)	**0.17 (4.42)**	0.82 (0.05)	4.6 (4.72)
GPP:												
TrEF	**0.26 (0.06)**	4.62 (7.33)	**0.26 (0.04)**	**-1.15 (6.39)**	0.27 (0.03)	-5.94 (5.66)	0.27 (0.03)	-5.03 (5.76)	0.27 (0.03)	-6.44 (5.6)	0.29 (0.04)	-12.6 (0.46)
TeBEF	0.46 (0.04)	**-5.88 (6.21)**	0.41 (0.04)	-8.58 (7.28)	0.42 (0.04)	-9.48 (6.64)	0.42 (0.04)	-9.56 (6.57)	0.4 (0.04)	-6.45 (6.84)	**0.38 (0.03)**	-13.58 (5.99)
TeBDF	0.58 (0.07)	3.95 (4.57)	**0.55 (0.07)**	-0.51 (4.27)	0.56 (0.07)	-0.66 (4.35)	0.56 (0.07)	-0.6 (4.3)	0.55 (0.07)	**-0.22 (4.16)**	0.58 (0.07)	-7.97 (3.63)
CEF	0.51 (0.03)	2.31 (3.6)	0.46 (0.03)	-3.87 (3.72)	0.48 (0.03)	-3.3 (3.88)	0.48 (0.03)	-3.5 (3.89)	0.46 (0.03)	**-1.08 (3.49)**	**0.45 (0.03)**	-6.64 (3.06)
TrS	**1.13 (0.03)**	-38.43 (24.14)	1.24 (0.08)	-47.32 (28.05)	1.26 (0.11)	-42.59 (32.16)	1.32 (0.14)	-42.45 (32.67)	1.21 (0.12)	-29.39 (29.04)	1.21 (0.1)	**-29.35 (32.06)**
TeS	0.59 (0.06)	**-15.09 (7.48)**	0.52 (0.05)	-18.99 (8.96)	0.54 (0.05)	-20.02 (8.66)	0.55 (0.05)	-20.75 (8.17)	**0.5 (0.04)**	-15.84 (8.05)	0.52 (0.04)	-15.13 (5.26)
TeH	1.08 (0.4)	37.79 (17.08)	1 (0.4)	30.6 (16.98)	1 (0.4)	31.01 (17.08)	**0.99 (0.39)**	30.26 (16.41)	1.02 (0.41)	32.84 (17.85)	1.05 (0.38)	**28.14 (15.84)**
All sites	0.66 (0.09)	6.29 (4.65)	**0.62 (0.09)**	0.64 (4.66)	0.63 (0.09)	0.72 (4.71)	0.63 (0.09)	**0.52 (4.6)**	**0.62 (0.09)**	3.07 (4.66)	0.63 (0.09)	-2.38 (4.3)

Values represent PFT-means (± standard errors). Measures are calculated based on daily model outputs. The best model for each measure and PFT is shown in bold. For PFT-abbreviations and number of sites in each group see Fig. 5.

4 Discussion

4.1 Model performance

The inclusion of a stomatal response mechanism to atmospheric humidity leads to significant improvements in model performance. Interestingly, while the inclusion of the VPD response causes substantial changes in water and carbon fluxes for almost all sites, differences between the model versions which are based on a coupled photosynthesis-stomatal conductance scheme are rather low. The different response functions embedded in JSBACH show different sensitivities of stomatal closure to an increase in VPD. This constitutes a great difference in G_c between the alternative models and the standard model; however, differences between the alternative models are marginal over a wide range of VPD values (Fig. 2). Only the BETHY model shows significant deviations for G_c compared to the other models. Since the model shows weak performance in ecosystems with a significant fraction of grasslands, poor parameterization might be seen as a reason, since parameter values assigned to C3 and C4 grasses are probably too high (Tab. 1). Additionally, observed differences between models under certain conditions (e.g. low VPD) are often compensated by the opposite pattern under contrasting conditions (e.g. high VPD). The USM for instance consistently predicts lower g_s under low VPD-conditions but also gives higher predictions under high VPD compared to the other models, while for the Friend model the opposite is the case (Fig. 5). A similar behavior can also be observed for daily (Fig. 4), and annual (Fig. H1) time series. Consequently, this leads to small total differences (Fig. 8). Since VPD varies significantly over the course of a day and between seasons, such compensating effects are likely to blur differences that exist at particular conditions. Indeed, significant variations between the model versions can not be detected if sites are grouped into climate groups (results not shown). The results indicate a clear improvement for all climate zones as model performance improves regardless of the mean growing season VPD, a quantity calculated to describe the influence of atmospheric demand on plant physiology (Fig. 9). The results demonstrate that the effect of stomatal closure in response to atmospheric humidity is important for all ecosystems, and plays a decisive role even under conditions of low or intermediate atmospheric drought.

One further possible reason for the low variability between the models can be seen in the limitations of the flux data. Eddy covariance measurements are subject to random and systematic errors, and therefore show high uncertainties as well as noise (Williams et al., 2009; Richardson et al., 2012). While the effect of random errors might be low for conditions of low VPD where many data are available, larger effects might occur under conditions of high VPD, were data availability is scarce. GPP and G_c further represent derived data that are again based on models, which adds further uncertainties. G_c for instance is based on the inversion of the Penman-Monteith equation, which assumes a closed energy balance and which requires an estimation of G_a, which is again based on meteorological data (Appendix E). Considering all possible uncertainties, the interpretation of minor differences between the models appears inappropriate. Moreover, some PFTs in this study are represented by a small number of stations, which are unlikely to adequately represent an entire biome. In general, the embedded process representations improve model performance with regard to ET and GPP for almost all PFTs. Obviously, larger differences occur in the global simulations, however a PFT-specific analysis for the global simulations was not conducted.

In this study, conditions of severe soil water stress are excluded (Appendix D.2), but minor effects from soil moisture are still possible, especially since soil moisture filters are only applied to the flux data, not to the modeled fluxes. Hence, under certain circumstances the model simulates soil water stress and thus reduced g_s even for periods considered as non-water-stressed in this

study. However, since soil moisture stress is likely to affect all models in a similar way, possible effects should have minor consequences for the results. An exception to this might be ecosystems characterized by seasonal water stress, like savannas or temperate broadleaf forests. For example, a highly overestimated net assimilation during summer drought possibly affects conditions several months later due to higher water use in the dry period. Therefore, an adequate treatment of soil water stress is necessary to exclude possible confounding effects from soil moisture (section 4.4).

4.2 The role of coupling to the atmosphere

The models evaluated in this study were developed and tested primarily by means of gas exchange experiments at the leaf level, where environmental factors are well controlled (Ball et al., 1987; Leuning, 1995). Stomatal aperture is then modeled in response to the environment close to the leaf surface, and leaf boundary layer conductance is held large. Under such conditions, leaves can be considered well coupled to the surrounding air, and both transpiration and photosynthesis can be assumed to be almost entirely controlled by stomata (Jarvis, 1986). In this study, fluxes are simulated at the ecosystem scale, and meteorological variables serving as model inputs such as atmospheric humidity and temperature are measured some distance above the canopy. However, meteorological conditions near the leaf surface can deviate largely from those in the free air stream (McNaughton and Jarvis, 1991). Grantz and Meinzer (1990) for instance found that VPD at the leaf surface may deviate from that in the atmosphere above by more than 1 kPa in croplands. The strength of this deviation depends on the degree of coupling between the vegetation and the atmosphere, which again is determined by the ratio of G_c to G_a (Appendix F), where G_a is dependent on wind speed, atmospheric stability, but also on plant structural properties such as vegetation height or density (Kelliher et al., 1993). The models applied in this study were not adjusted for application at the canopy scale, which means that stomata in the model respond to the VPD measured some meters away from the canopy, whereas the "true" driving force for transpiration is the VPD in the immediate surrounding of the leaf. In the study by Launiainen et al. (2011), the Ball-Berry and Leuning models have been shown to respond well to changes in VPD at the canopy scale, for both with and without adjustment of VPD to leaf conditions. However, the study was conducted in a coniferous forest, which is in most cases well coupled to the atmosphere (McNaughton and Jarvis, 1991). A similar study conducted in croplands emphasized the need to correct the measured VPD in the free atmosphere for the effect of decoupling (Grantz and Meinzer, 1990).

The effect of coupling has been shown to influence the G_c - ET relation considerably. This effect might cause a poor representation of water fluxes, even if G_c is accurately modeled. McNaughton and Jarvis (1991) for instance proposed negative feedbacks at the leaf and canopy scale in case of a low G_a. Low G_a and therefore high humidity and temperatures in the immediate surroundings of the leaf compared to the free air stream reduce transpiration. This effect diminishes the sensitivity of transpiration to changes in g_s, since even high g_s does not increase transpiration if humidity near the leaf surface is high. Indeed, studies have shown that vegetation types characterized by a high degree of coupling (e.g. coniferous forests) show higher sensitivities of ET to changes in G_c than ecosystems with a high decoupling (e.g. grasslands) (Kelliher et al., 1993). Computed coupling coefficients for different PFTs in this study (Fig. F1) illustrate the differences between vegetation types. The mentioned reduced sensitivity of ET to changes in G_c becomes apparent as even large changes in G_c between the standard model and the alternative models does not lead to comparable changes in the transpiration flux for PFTs characterized by poor coupling to the

atmosphere, such as grasslands or tropical rainforests. For example, a comparable reduction in G_c compared to the standard model for tropical rainforests and coniferous forests does not result in the same degree of reduction in ET for both ecosystems. Instead, ET is much more sensitive to changes in G_c in coniferous forests than in tropical rainforests. The effect is even more pronounced for grasslands (Figs. 5,6). Such negative feedbacks were considered to strengthen with an increase in scale by Jarvis (1986), so that stomatal processes were supposed to play only a marginal role in the water flux over continents. Later modeling studies (Friend and Cox, 1995; Friend and Kiang, 2005), however, indicated that stomatal control has a major impact on regional transpiration, since positive feedbacks with atmospheric humidity compensate the negative feedback mechanisms described beforehand. According to Friend and Kiang (2005), reduced transpiration due to decoupling effects would increase the humidity deficit in the atmosphere and consequently increase transpiration. In this study, global simulations were run offline (i.e. vegetation is decoupled from the atmosphere), and vegetation-climate feedbacks are therefore largely neglected, which hinders a detailed investigation of the role of stomatal regulation for regional water fluxes.
In any case, while at the leaf level the accurate modeling of stomatal conductance depends on the specific functional relationship deployed (e.g. Leuning, 1995) as well as on the measure for atmospheric humidity (Aphalo and Jarvis, 1991) those factors seem to be less relevant at large spatial scales, even though G_c has been shown to be sensitive to changes in atmospheric humidity (Grantz and Meinzer, 1990; Launiainen et al., 2011). Additional confounding factors such as radiation and vegetation-atmosphere feedback mechanisms lead to a less clear relation between G_c and the exchange of water and CO_2 at the canopy scale (McNaughton and Jarvis, 1991). Besides confounding physical effects, physiological variations between species have to be considered at the canopy scale. The synthesis study by Oren et al. (1999) revealed high intra- and interspecific variations of the stomatal sensitivity to increasing VPD. The consideration of such differences and its translation into mathematical representations applicable in global climate models, however, constitutes a big challenge.

4.3 Model parameterization

The results did not clearly support any of the models, neither for particular ecosystems, nor at the global scale. However, all models might benefit from an improved model parameterization. The common parameter for photosynthesis-stomatal conductance models is the slope parameter g_1, which represents stomatal sensitivity to the combined factors of A_n, C_a and atmospheric humidity (Ball et al., 1987). In this study, g_1 was treated as a global constant, which varies with water stress, but not with climatic conditions or plant functional traits. The original Ball-Berry model was indeed developed for a wide range of conditions (Ball et al., 1987) and gave accurate results for different environments (Buckley and Mott, 2013). Further studies (Xu and Baldocchi, 2003) found a constant slope under extremely high air temperatures and severe water stress as well as for different leaf ages. This proposed conservative behavior of g_1 across environmental conditions is contentious, since other studies found considerable variations with environment such as growth temperature or light conditions (Bunce, 1998) or over the course of the growing season (Valentini et al., 1995; Launiainen et al., 2011). In any case, it is well known that the slope parameter varies between species (Ball et al., 1987). However, the Ball-Berry-type models fail to account for such behavioral differences between individuals and species, unless a correct parameterization is achieved (Gao et al., 2002), which appears to be unfeasible at larger scales. In current global models, possible parameter variations based on plant properties can only be accounted for if they differ between PFTs, the highest aggregation level employed in LSMs. It is still unclear if param-

eter variations can be attributed to differences in plant properties, on which the PFT-concept is based on, though first studies revealed differences between PFTs (Manzoni et al., 2011). Parameter values estimated from flux data in this study showed differences across PFTs (Fig. G2), but any conclusions remain specious until a sound relation between plant functional traits and parameter values can be established, which is additionally reconcilable with the PFT-concept. The latter point seems unclear. Fig. G2 shows high variations within PFTs, which can be partly attributed to the noise in the flux data (Fig. G1 shows high scatter and a low R^2 despite the application of a data filtering procedure), but which also reflect large differences between sites representing the same ecosystem type. Large variations for related species were also found by (Bowden and Bauerle, 2008), who determined species-specific g_1 values that differed by the factor of 3 for deciduous broadleaf trees. Consequently, parameter estimation on a PFT-basis might not be a promising approach for current global climate models, but further investigations are needed.

Those difficulties in model parameterization are mainly due to the empirical nature of stomatal conductance-photosynthesis models. g_1 comes without a theoretical explanation, which hinders the understanding of how parameters vary with climate or species (Medlyn et al., 2011). The unified stomatal model (USM) was developed to overcome this drawback (Medlyn et al., 2011). The USM provides a theoretical underpinning of the slope parameter, such that it is proportional to the marginal water cost of plant carbon uptake λ and to Γ^*, quantities that are known to vary with environmental conditions. While Γ^* is known to increase with growth temperature (Bernacchi et al., 2001), the variation of λ among species and growth conditions is not yet clear (Medlyn et al., 2011) and subject of current and future research. Theory suggests that species in sub-humid regions which have to endure unfavorable climatic periods require more carbon investments in cavitation-resistant tissues or xerophytic leaves and consequently show lower values for λ and g_1 (Héroult et al., 2013). In fact, soil moisture deficit seems to play an important role for the value of λ due to the above mentioned reasons, and determined values for λ were lower for species in dry than in humid environments (Manzoni et al., 2011; Héroult et al., 2013). To summarize, the USM has the capability of overcoming difficulties in parameterization by the provision of a theoretical framework for stomatal modeling. Due to its analogy to the Ball-Berry type models (Medlyn et al., 2011) which was confirmed in this study (Fig. G2: estimated slopes across PFTs varied in the same manner for both the Ball-Berry and the USM), insights gained from the USM also be used for empirical stomatal models and ultimately provide parameter distributions in space and time, provided that stomata operate optimally as predicted by the USM, which is still under debate (Medlyn et al., 2013).

The parameter g_1 is further inversely proportional to the intrinsic WUE at the leaf level (Héroult et al., 2013). This relation could be useful to improve the representation of water-carbon interactions in LSMs, if WUE at the canopy scale changes in proportion to g_1 as theory suggests. The slopes estimated in this study (Fig. G2) were in most cases larger than the default value in the model. According to theory, model runs with higher g_1 parameters would consequently lead to reduced WUE, which would be an improvement for most, but not all PFTs.

Model parameterization was also the main limitation for the application of the BETHY model. In principle, the approach has the great advantage of modeling the stomatal response to variations of atmospheric drought and soil water stress simultaneously. The model further appears to be suitable for use in GCMs due to its simplicity. Only one parameter, representing the whole-plant hydraulic conductivity (Knorr, 2000), is required. However, information about plant hydraulic properties at the PFT-level is sparse or not available in the required unit (Hickler et al., 2006), which hampers the use of the BETHY model in LSMs. Hence, further investigations are needed

which relate plant functional properties to transpiration. One promising approach in this direction is given by Santiago et al. (2004) or Brodribb et al. (2005) who investigated the relation between photosynthesis, stomatal conductance, and hydraulic conductivity in leaves, a concept which appears to be applicable in LSMs. However, since this approach is not widely tested, its validity has first to be confirmed by e.g. experimental studies at different scales.
The Ball-Berry and Leuning approach did not show large differences in this study, but represent stomatal response to atmospheric humidity with a different degree of complexity. The Leuning model includes a third parameter D_0, which adjusts the stomatal sensitivity to changes in VPD (Leuning, 1995). Since the determined values of D_0 vary largely between species (Leuning, 1995; Medlyn et al., 2011; Héroult et al., 2013), the spatial variability of this parameter cannot be accounted for in current LSMs. Therefore, the additional complexity is of no use for global simulations, unless spatial parameter estimates are available.

4.4 Effects of soil water stress

The poor model performance in arid and semiarid ecosystems underlines the importance of accurately representing the effect of soil water stress in coupled photosynthesis-stomatal conductance models (Egea et al., 2011). Applying a normalized soil moisture dependent stress function solely to g_s and thus reducing the slope parameter g_1 in the models proved to be insufficient for capturing the response of water and carbon fluxes to soil water scarcity at the ecosystem level. This finding is consistent with outcomes of modeling studies at the leaf (Misson et al., 2010; Egea et al., 2011; Zhou et al., 2013) and ecosystem scale (Keenan et al., 2009; Keenan et al., 2010). In fact, these studies have shown that non-stomatal limitations to A_n need to be included when modeling the effects of drought on photosynthesis and transpiration. Proposed non-stomatal mechanisms operate either directly on leaf biochemistry (via reduced V_{cmax} and/or J_{max} (e.g. Parry et al., 2002)) or through a decrease in mesophyll conductance along with a decrease in soil water deficit (Flexas et al., 2012). Both processes ultimately lead to a reduction in carboxylation capacity (V_{cmax}), either directly or indirectly (Zhou et al., 2013). The relative importance of these processes for different degrees of soil water stress is still under debate (Grassi and Magnani, 2005; Misson et al., 2010; Egea et al., 2011) and remains a subject for future research. Regardless of the underlying mechanism, the necessity of reducing photosynthetic capacity in periods of drought was underlined in this study by the fact that solely reducing the slope parameter g_1 leads to a severe overproduction in arid and semi-arid regions of the world (Figs. 11,13). This erroneous model behavior is most likely due to the numerical instability of the applied algorithm resulting from the missing process component described above.
One further aspect to investigate with regard to soil moisture is how g_s, photosynthetic capacity, and mesophyll conductance respond to a decline in soil moisture. In JSBACH, a linear decline of g_s is presupposed (Eqs. 15,16), however studies have indicated that the sensitivity to soil moisture is not linear in its functional form (Misson et al., 2010), or differs between stomatal and non-stomatal processes, as well as across PFTs (Zhou et al., 2013). Another mechanism which might serve as an explanation for the enhanced productivity in seasonally dry regions is a seasonal shift in the growing season as a consequence of stomatal closure. This leads to reduced transpiration in the early growing season and consequently to a prolonged vegetation activity resulting from the higher water availability in the dry period. Even though this mechanism is likely to effect the seasonal dynamics of plant productivity, especially in Mediterranean ecosystems (Fig. H1), it appears highly unlikely that the large increase in productivity as observed in the global simulations can be attributed solely to shifts in the seasonal cycle.

5 Conclusions

The effect of atmospheric humidity on stomatal conductance has significant consequences for carbon and water fluxes, not only at the leaf level, but also for simulations at the ecosystem and global scale. The stomatal response to atmospheric humidity is therefore a process which needs to be considered in global climate models. Canopy conductance is sensitive to changes in VPD regardless of climatic conditions and plant functional types. The response of transpiration, however, differs among PFTs, most likely due to the effect of decoupling between the vegetation and the atmosphere. The negligible differences between the model versions at the ecosystem scale support the use of simple stomatal conductance schemes in LSMs. Hence, due to its simplicity and its capability of showing good results for all PFTs, the Ball-Berry model can be considered as the best option for climate models as long as no detailed knowledge on model parameters is available. Estimated parameter values from flux data showed high variability between sites and considerable variations from the values currently used in the models. Since parameters were treated as global constants and possible variations with growth conditions or plant traits could not be accounted for, model parameterization can be considered as a major restriction to model performance. Certainly, an advanced knowledge on the spatial distribution and temporal dynamics of parameter values would help to achieve an improved representation of carbon and water interactions in global models. The interplay between stomatal conductance and photosynthesis critically depends on how the effect of soil moisture on plant physiology is considered in the model.

References

Ammann, C., Flechard, C., Leifeld, J, Neftel, A, and Fuhrer, J (2007). The carbon budget of newly established temperate grassland depends on management intensity. *Agriculture, ecosystems & environment* 121, 5–20.

Aphalo, P. and Jarvis, P. (1991). Do stomata respond to relative humidity? *Plant, Cell & Environment* 14, 127–132.

— (1993). An analysis of Ball's empirical model of stomatal conductance. *Annals of Botany* 72, 321–327.

Araújo, A., Nobre, A., Kruijt, B, Elbers, J., Dallarosa, R, Stefani, P, Von Randow, C, Manzi, A., Culf, A., Gash, J., et al. (2002). Comparative measurements of carbon dioxide fluxes from two nearby towers in a central Amazonian rainforest: The Manaus LBA site. *Journal of Geophysical Research-Atmosphere* 107, 8090.

Archibald, S., Nickless, A, Govender, N, Scholes, R., and Lehsten, V. (2010). Climate and the inter-annual variability of fire in southern Africa: a meta-analysis using long-term field data and satellite-derived burnt area data. *Global Ecology and Biogeography* 19, 794–809.

Baldocchi, D., Falge, E., Gu, L., Olson, R., Hollinger, D., Running, S., Anthoni, P., Bernhofer, C., Davis, K., Evans, R., et al. (2001). FLUXNET: A new tool to study the temporal and spatial variability of ecosystem-scale carbon dioxide, water vapor, and energy flux densities. *Bulletin of the American Meteorological Society* 82, 2415–2434.

Ball, J. T., Woodrow, I. E., and Berry, J. A. (1987). A model predicting stomatal conductance and its contribution to the control of photosynthesis under different environmental conditions. In: *Progress in photosynthesis research*. Ed. by J Biggins. Martinus Nijhoff Publishers, Dordrecht, Netherlands, 221–224.

Beer, C, Ciais, P, Reichstein, M, Baldocchi, D, Law, B., Papale, D, Soussana, J.-F., Ammann, C, Buchmann, N, Frank, D, et al. (2009). Temporal and among-site variability of inherent water use efficiency at the ecosystem level. *Global biogeochemical cycles* 23.

Beer, C., Reichstein, M., Tomelleri, E., Ciais, P., Jung, M., Carvalhais, N., Rödenbeck, C., Arain, M. A., Baldocchi, D., Bonan, G. B., et al. (2010). Terrestrial gross carbon dioxide uptake: global distribution and covariation with climate. *Science* 329, 834–838.

Berbigier, P., Bonnefond, J.-M., and Mellmann, P. (2001). CO_2 and water vapour fluxes for 2 years above Euroflux forest site. *Agricultural and Forest Meteorology* 108, 183–197.

Bergeron, O., Margolis, H. A., Black, T. A., Coursolle, C., Dunn, A. L., Barr, A. G., and Wofsy, S. C. (2007). Comparison of carbon dioxide fluxes over three boreal black spruce forests in Canada. *Global Change Biology* 13, 89–107.

Beringer, J., Hutley, L. B., Hacker, J. M., Neininger, B., and Paw U, K. T. (2011). Patterns and processes of carbon, water and energy cycles across northern Australian landscapes: From point to region. *Agricultural and Forest Meteorology* 151, 1409–1416.

Bernacchi, C., Singsaas, E., Pimentel, C, Portis Jr, A., and Long, S. (2001). Improved temperature response functions for models of Rubisco-limited photosynthesis. *Plant, Cell & Environment* 24, 253–259.

Berry, J. A., Beerling, D. J., and Franks, P. J. (2010). Stomata: key players in the earth system, past and present. *Current opinion in plant biology* 13, 232–239.

Bonan, G. (2008). *Ecological Climatology*. Cambridge University Press, New York.

Bowden, J. D. and Bauerle, W. L. (2008). Measuring and modeling the variation in species-specific transpiration in temperate deciduous hardwoods. *Tree physiology* 28, 1675–1683.

Brodribb, T. J., Holbrook, N. M., Zwieniecki, M. A., and Palma, B. (2005). Leaf hydraulic capacity in ferns, conifers and angiosperms: impacts on photosynthetic maxima. *New phytologist* 165, 839–846.

Buckley, T. N. and Mott, K. A. (2013). Modelling stomatal conductance in response to environmental factors. *Plant, cell & environment* 36, 1691–1699.

Bunce, J. A. (1998). Effects of environment during growth on the sensitivity of leaf conductance to changes in humidity. *Global Change Biology* 4, 269–274.

Carrara, A., Janssens, I. A., Curiel Yuste, J., and Ceulemans, R. (2004). Seasonal changes in photosynthesis, respiration and NEE of a mixed temperate forest. *Agricultural and Forest Meteorology* 126, 15–31.

Chiesi, M, Maselli, F, Bindi, M, Fibbi, L, Cherubini, P, Arlotta, E, Tirone, G, Matteucci, G, and Seufert, G (2005). Modelling carbon budget of Mediterranean forests using ground and remote sensing measurements. *Agricultural and Forest Meteorology* 135, 22–34.

Choudhury, B. and Monteith, J. (1988). A four-layer model for the heat budget of homogeneous land surfaces. *Quarterly Journal of the Royal Meteorological Society* 114, 373–398.

Clark, K. L., Gholz, H. L., Moncrieff, J. B., Cropley, F., and Loescher, H. W. (1999). Environmental controls over net exchanges of carbon dioxide from contrasting Florida ecosystems. *Ecological Applications* 9, 936–948.

Cleugh, H. A., Leuning, R., Mu, Q., and Running, S. W. (2007). Regional evaporation estimates from flux tower and MODIS satellite data. *Remote Sensing of Environment* 106, 285–304.

Collatz, G. J., Ball, J. T., Grivet, C., and Berry, J. A. (1991). Physiological and environmental regulation of stomatal conductance, photosynthesis and transpiration: a model that includes a laminar boundary layer. *Agricultural and Forest Meteorology* 54, 107–136.

Collatz, G. J., Ribas-Carbo, M, and Berry, J. (1992). Coupled photosynthesis-stomatal conductance model for leaves of C4 plants. *Functional Plant Biology* 19, 519–538.

Cook, B. D., Davis, K. J., Wang, W., Desai, A., Berger, B. W., Teclaw, R. M., Martin, J. G., Bolstad, P. V., Bakwin, P. S., Yi, C., et al. (2004). Carbon exchange and venting anomalies in an upland deciduous forest in northern Wisconsin, USA. *Agricultural and Forest Meteorology* 126, 271–295.

Cowan, I. (1965). Transport of water in the soil-plant-atmosphere system. *Journal of Applied Ecology* 2, 221–239.

Cowan, I. and Farquhar, G. (1977). Stomatal function in relation to leaf metabolism and environment. In: *Symposia of the Society for Experimental Biology*. Vol. 31, 471–505.

Dai, A. (2011). Drought under global warming: a review. *Wiley Interdisciplinary Reviews: Climate Change* 2, 45–65.

Damour, G., Simonneau, T., Cochard, H., and Urban, L. (2010). An overview of models of stomatal conductance at the leaf level. *Plant, Cell & Environment* 33, 1419–1438.

Davis, K. J., Bakwin, P. S., Yi, C., Berger, B. W., Zhao, C., Teclaw, R. M., and Isebrands, J. (2003). The annual cycles of CO_2 and H_2O exchange over a northern mixed forest as observed from a very tall tower. *Global Change Biology* 9, 1278–1293.

Dee, D., Uppala, S., Simmons, A., Berrisford, P, Poli, P, Kobayashi, S, Andrae, U, Balmaseda, M., Balsamo, G, Bauer, P, et al. (2011). The ERA-Interim reanalysis: Configuration and performance of the data assimilation system. *Quarterly Journal of the Royal Meteorological Society* 137, 553–597.

Desai, A. R., Bolstad, P. V., Cook, B. D., Davis, K. J., and Carey, E. V. (2005). Comparing net ecosystem exchange of carbon dioxide between an old-growth and mature forest in the upper Midwest, USA. *Agricultural and Forest Meteorology* 128, 33–55.

Dirks, B. and Hensen, A (1999). Surface conductance and energy exchange in an intensively managed peat pasture. *Climate Research* 12, 29–37.

Dolman, A., Moors, E., and Elbers, J. (2002). The carbon uptake of a mid latitude pine forest growing on sandy soil. *Agricultural and Forest Meteorology* 111, 157–170.

Dunn, A. L., Barford, C. C., Wofsy, S. C., Goulden, M. L., and Daube, B. C. (2007). A long-term record of carbon exchange in a boreal black spruce forest: Means, responses to interannual variability, and decadal trends. *Global Change Biology* 13, 577–590.

Egea, G., Verhoef, A., and Vidale, P. L. (2011). Towards an improved and more flexible representation of water stress in coupled photosynthesis–stomatal conductance models. *Agricultural and Forest Meteorology* 151, 1370–1384.

Farquhar, G. (1988). Models relating subcellular effects of temperature to whole plant responses. In: *Symposia of the Society for Experimental Biology*. Vol. 42, 395.

Farquhar, G., Caemmerer, S. v. von, and Berry, J. (1980). A biochemical model of photosynthetic CO_2 assimilation in leaves of C3 species. *Planta* 149, 78–90.

Federer, C. A. (1982). Transpirational supply and demand: plant, soil, and atmospheric effects evaluated by simulation. *Water Resources Research* 18, 355–362.

Field, C., Jackson, R., and Mooney, H. (1995). Stomatal responses to increased CO_2: implications from the plant to the global scale. *Plant, Cell & Environment* 18, 1214–1225.

Flexas, J., Barbour, M. M., Brendel, O., Cabrera, H. M., Carriquí, M., Díaz-Espejo, A., Douthe, C., Dreyer, E., Ferrio, J. P., Gago, J., et al. (2012). Mesophyll diffusion conductance to CO_2: An unappreciated central player in photosynthesis. *Plant Science* 193, 70–84.

Friedl, M. A., Sulla-Menashe, D., Tan, B., Schneider, A., Ramankutty, N., Sibley, A., and Huang, X. (2010). MODIS Collection 5 global land cover: Algorithm refinements and characterization of new datasets. *Remote Sensing of Environment* 114, 168–182.

Friend, A. D. and Cox, P. M. (1995). Modelling the effects of atmospheric CO_2 on vegetation-atmosphere interactions. *Agricultural and Forest Meteorology* 73, 285–295.

Friend, A. D. and Kiang, N. Y. (2005). Land Surface Model Development for the GISS GCM: Effects of Improved Canopy Physiology on Simulated Climate. *Journal of Climate* 18, 2883–2902.

Gao, Q, Zhao, P, Zeng, X, Cai, X, and Shen, W (2002). A model of stomatal conductance to quantify the relationship between leaf transpiration, microclimate and soil water stress. *Plant, Cell & Environment* 25, 1373–1381.

Gedney, N., Cox, P., Betts, R., Boucher, O, Huntingford, C, and Stott, P. (2006). Detection of a direct carbon dioxide effect in continental river runoff records. *Nature* 439, 835–838.

Gilmanov, T., Soussana, J., Aires, L, Allard, V, Ammann, C., Balzarolo, M, Barcza, Z, Bernhofer, C, Campbell, C., Cernusca, A, et al. (2007). Partitioning European grassland net ecosystem CO_2 exchange into gross primary productivity and ecosystem respiration using light response function analysis. *Agriculture, ecosystems & environment* 121, 93–120.

Giorgetta, M. A., Jungclaus, J., Reick, C. H., Legutke, S., Bader, J., Böttinger, M., Brovkin, V., Crueger, T., Esch, M., Fieg, K., et al. (2013). Climate and carbon cycle changes from 1850 to 2100 in MPI-ESM simulations for the Coupled Model Intercomparison Project phase 5. *Journal of Advances in Modeling Earth Systems* 5, 572–597.

Goldstein, A., Hultman, N., Fracheboud, J., Bauer, M., Panek, J., Xu, M, Qi, Y, Guenther, A., and Baugh, W (2000). Effects of climate variability on the carbon dioxide, water, and sensible heat fluxes above a ponderosa pine plantation in the Sierra Nevada (CA). *Agricultural and Forest Meteorology* 101, 113–129.

Granier, A, Ceschia, E, Damesin, C, Dufrêne, E, Epron, D, Gross, P, Lebaube, S, Le Dantec, V, Le Goff, N, Lemoine, D., et al. (2000). The carbon balance of a young beech forest. *Functional ecology* 14, 312–325.

Grantz, D. and Meinzer, F. (1990). Stomatal response to humidity in a sugarcane field: simultaneous porometric and micrometeorological measurements. *Plant, Cell & Environment* 13, 27–37.

Grassi, G. and Magnani, F. (2005). Stomatal, mesophyll conductance and biochemical limitations to photosynthesis as affected by drought and leaf ontogeny in ash and oak trees. *Plant, Cell & Environment* 28, 834–849.

Grelle, A, Lundberg, A, Lindroth, A, Moren, A.-S., and Cienciala, E (1997). Evaporation components of a boreal forest: variations during the growing season. *Journal of Hydrology* 197, 70–87.

Grünwald, T. and Bernhofer, C. (2007). A decade of carbon, water and energy flux measurements of an old spruce forest at the Anchor Station Tharandt. *Tellus B* 59, 387–396.

Grünzweig, J., Lin, T, Rotenberg, E, Schwartz, A, and Yakir, D (2003). Carbon sequestration in arid-land forest. *Global Change Biology* 9, 791–799.

Gu, L., Meyers, T., Pallardy, S. G., Hanson, P. J., Yang, B., Heuer, M., Hosman, K. P., Riggs, J. S., Sluss, D., and Wullschleger, S. D. (2006). Direct and indirect effects of atmospheric conditions and soil moisture on surface energy partitioning revealed by a prolonged drought at a temperate forest site. *Journal of Geophysical Research-Atmosphere* 111, D16102.

Hagemann, S. and Stacke, T. (2014). Impact of the soil hydrology scheme on simulated soil moisture memory. *Climate Dynamics*, 1–20.

Hansen, J, Russell, G, Rind, D, Stone, P, Lacis, A, Lebedeff, S, Ruedy, R, and Travis, L (1983). Efficient three-dimensional global models for climate studies: Models I and II. *Monthly Weather Review* 111, 609–662.

Hartmann, D. et al. (2013). Observations: Atmosphere and Surface. In: *Climate Change 2013: The Physical Science Basis. Contribution of Working Group I to the Fifth Assessment Report of the Intergovernmental Panel on Climate Change*. Cambridge University Press, 159–254.

Héroult, A., Lin, Y.-S., Bourne, A., Medlyn, B. E., and Ellsworth, D. S. (2013). Optimal stomatal conductance in relation to photosynthesis in climatically contrasting Eucalyptus species under drought. *Plant, cell & environment* 36, 262–274.

Hickler, T., Prentice, I. C., Smith, B., Sykes, M. T., and Zaehle, S. (2006). Implementing plant hydraulic architecture within the LPJ Dynamic Global Vegetation Model. *Global Ecology and Biogeography* 15, 567–577.

Hirano, T., Segah, H., Harada, T., Limin, S., June, T., Hirata, R., and Osaki, M. (2007). Carbon dioxide balance of a tropical peat swamp forest in Kalimantan, Indonesia. *Global Change Biology* 13, 412–425.

Hollinger, D., Goltz, S., Davidson, E., Lee, J., Tu, K, and Valentine, H. (1999). Seasonal patterns and environmental control of carbon dioxide and water vapour exchange in an ecotonal boreal forest. *Global Change Biology* 5, 891–902.

Jacobs, C., Jacobs, A., Bosveld, F., Hendriks, D., Hensen, A, Kroon, P., Moors, E., Nol, L, Schrier-Uijl, A, Veenendaal, E., et al. (2007). Variability of annual CO_2 exchange from Dutch grasslands. *Biogeosciences* 4, 803–816.

Janssen, P. and Heuberger, P. (1995). Calibration of process-oriented models. *Ecological Modelling* 83, 55–66.

Jarvis, P. (1976). The interpretation of the variations in leaf water potential and stomatal conductance found in canopies in the field. *Philosophical Transactions of the Royal Society of London. B, Biological Sciences* 273, 593–610.

Jarvis, P. (1986). Coupling of carbon and water interactions in forest stands. *Tree physiology* 2, 347–368.

Jung, M, Maire, G. L., Zaehle, S, Luyssaert, S, Vetter, M, Churkina, G, Ciais, P, Viovy, N, and Reichstein, M (2007). Assessing the ability of three land ecosystem models to simulate gross carbon uptake of forests from boreal to Mediterranean climate in Europe. *Biogeosciences* 4, 647–656.

Jung, M., Reichstein, M., Margolis, H. A., Cescatti, A., Richardson, A. D., Arain, M. A., Arneth, A., Bernhofer, C., Bonal, D., Chen, J., et al. (2011). Global patterns of land-atmosphere fluxes of carbon dioxide, latent heat, and sensible heat derived from eddy covariance, satellite, and meteorological observations. *Journal of Geophysical Research: Biogeosciences* 116, G00J07.

Katul, G., Manzoni, S., Palmroth, S., and Oren, R. (2010). A stomatal optimization theory to describe the effects of atmospheric CO_2 on leaf photosynthesis and transpiration. *Annals of Botany* 105, 431–442.

Katul, G. G., Palmroth, S., and Oren, R. (2009). Leaf stomatal responses to vapour pressure deficit under current and CO_2-enriched atmosphere explained by the economics of gas exchange. *Plant, cell & environment* 32, 968–979.

Keenan, T, Garcia, R, Friend, A., Zaehle, S, Gracia, C, and Sabate, S (2009). Improved understanding of drought controls on seasonal variation in Mediterranean forest canopy CO_2 and water fluxes through combined in situ measurements and ecosystem modelling. *Biogeosciences Discussions* 6, 2285–2329.

Keenan, T., Sabate, S., and Gracia, C. (2010). Soil water stress and coupled photosynthesis–conductance models: Bridging the gap between conflicting reports on the relative roles of stomatal, mesophyll conductance and biochemical limitations to photosynthesis. *Agricultural and Forest Meteorology* 150, 443–453.

Keenan, T. F., Hollinger, D. Y., Bohrer, G., Dragoni, D., Munger, J. W., Schmid, H. P., and Richardson, A. D. (2013). Increase in forest water-use efficiency as atmospheric carbon dioxide concentrations rise. *Nature* 499, 324–327.

Kelliher, F., Leuning, R, and Schulze, E. (1993). Evaporation and canopy characteristics of coniferous forests and grasslands. *Oecologia* 95, 153–163.

Knorr, W. (1997). Satellitengestützte Fernerkundung und Modellierung des Globalen CO_2-Austauschs der Landvegetation: Eine Synthese. PhD thesis. Max-Planck-Institut für Meteorologie Hamburg, Germany.

— (2000). Annual and interannual CO_2 exchanges of the terrestrial biosphere: Process-based simulations and uncertainties. *Global Ecology and Biogeography* 9, 225–252.

Kuglitsch, F., Reichstein, M, Beer, C, Carrara, A, Ceulemans, R, Granier, A, Janssens, I., Koestner, B, Lindroth, A, Loustau, D, et al. (2008). Characterisation of ecosystem water-use efficiency of european forests from eddy covariance measurements. *Biogeosciences Discussions* 5, 4481–4519.

Kutsch, W. L., Kolle, O., Rebmann, C., Knohl, A., Ziegler, W., and Schulze, E.-D. (2008). Advection and resulting CO_2 exchange uncertainty in a tall forest in central Germany. *Ecological Applications* 18, 1391–1405.

Lagergren, F., Lindroth, A., Dellwik, E., Ibrom, A., Lankreijer, H., Launiainen, S., Mölder, M., Kolari, P., Pilegaard, K., and Vesala, T. (2008). Biophysical controls on CO_2 fluxes of three northern forests based on long-term eddy covariance data. *Tellus B* 60, 143–152.

Launiainen, S., Katul, G. G., Kolari, P., Vesala, T., and Hari, P. (2011). Empirical and optimal stomatal controls on leaf and ecosystem level CO_2 and H_2 O exchange rates. *Agricultural and Forest Meteorology* 151, 1672–1689.

Law, B., Thornton, P., Irvine, J, Anthoni, P., and Van Tuyl, S (2001). Carbon storage and fluxes in ponderosa pine forests at different developmental stages. *Global Change Biology* 7, 755–777.

Leuning, R (1990). Modelling stomatal behaviour and and photosynthesis of Eucalyptus grandis. *Functional Plant Biology* 17, 159–175.

— (1995). A critical appraisal of a combined stomatal-photosynthesis model for C3 plants. *Plant, Cell & Environment* 18, 339–355.

Lindroth, A., Klemedtsson, L., Grelle, A., Weslien, P., and Langvall, O. (2008). Measurement of Net Ecosystem Exchange, Productivity and Respiration in Three Spruce Forests in Sweden Shows Unexpectedly Large Soil Carbon Losses. *Biogeochemistry*, 43–60.

Lohammar, T, Larsson, S, Linder, S, and Falk, S. (1980). FAST: Simulation models of gaseous exchange in Scots pine. *Ecological Bulletins*, 505–523.

Ma, S., Baldocchi, D. D., Xu, L., and Hehn, T. (2007). Inter-annual variability in carbon dioxide exchange of an oak/grass savanna and open grassland in California. *Agricultural and Forest Meteorology* 147, 157–171.

Manzoni, S., Vico, G., Katul, G., Fay, P. A., Polley, W., Palmroth, S., and Porporato, A. (2011). Optimizing stomatal conductance for maximum carbon gain under water stress: a meta-analysis across plant functional types and climates. *Functional Ecology* 25, 456–467.

Marcolla, B., Pitacco, A, and Cescatti, A (2003). Canopy architecture and turbulence structure in a coniferous forest. *Boundary-layer meteorology* 108, 39–59.

Martin, D., Beringer, J., Hutley, L. B., and McHugh, I. (2007). Carbon cycling in a mountain ash forest: analysis of below ground respiration. *Agricultural and Forest Meteorology* 147, 58–70.

Mascart, P., Taconet, O., Pinty, J.-P., and Mehrez, M. B. (1991). Canopy resistance formulation and its effect in mesoscale models: a HAPEX perspective. *Agricultural and Forest Meteorology* 54, 319–351.

McNaughton, K. and Jarvis, P. (1991). Effects of spatial scale on stomatal control of transpiration. *Agricultural and Forest Meteorology* 54, 279–302.

Medlyn, B. E., Duursma, R. A., Eamus, D., Ellsworth, D. S., Prentice, I. C., Barton, C. V., Crous, K. Y., Angelis, P. de, Freeman, M., and Wingate, L. (2011). Reconciling the optimal and empirical approaches to modelling stomatal conductance. *Global Change Biology* 17, 2134–2144.

Medlyn, B. E., Duursma, R. A., De Kauwe, M. G., and Prentice, I. C. (2013). The optimal stomatal response to atmospheric CO_2 concentration: Alternative solutions, alternative interpretations. *Agricultural and Forest Meteorology* 182, 200–203.

Migliavacca, M., Meroni, M., Manca, G., Matteucci, G., Montagnani, L., Grassi, G., Zenone, T., Teobaldelli, M., Goded, I., Colombo, R., et al. (2009). Seasonal and interannual patterns of carbon and water fluxes of a poplar plantation under peculiar eco-climatic conditions. *Agricultural and forest meteorology* 149, 1460–1476.

Misson, L., LIMOUSIN, J., Rodriguez, R., and Letts, M. G. (2010). Leaf physiological responses to extreme droughts in Mediterranean Quercus ilex forest. *Plant, cell & environment* 33, 1898–1910.

Mkhabela, M., Amiro, B., Barr, A., Black, T., Hawthorne, I, Kidston, J, McCaughey, J., Orchansky, A., Nesic, Z, Sass, A, et al. (2009). Comparison of carbon dynamics and water use efficiency following fire and harvesting in Canadian boreal forests. *Agricultural and Forest Meteorology* 149, 783–794.

Monteith, J. (1973). *Principles of Environmental Physics*. Edward Arnold.

Monteith, J. (1965). Evaporation and environment. In: *Symp. Soc. Exp. Biol.* Vol. 19, 4.

Morales, P., Sykes, M. T., Prentice, I. C., Smith, P., Smith, B., Bugmann, H., Zierl, B., Friedlingstein, P., Viovy, N., Sabate, S., et al. (2005). Comparing and evaluating process-based ecosystem model predictions of carbon and water fluxes in major European forest biomes. *Global Change Biology* 11, 2211–2233.

Mott, K. and Parkhurst, D. (1991). Stomatal responses to humidity in air and helox. *Plant, Cell & Environment* 14, 509–515.

Müller, B., Hirschi, M., Jimenez, C, Ciais, P, Dirmeyer, P., Dolman, A., Fisher, J., Jung, M, Ludwig, F, Maignan, F, et al. (2013). Benchmark products for land evapotranspiration: LandFlux-EVAL multi-dataset synthesis. *Hydrology & Earth System Sciences Discussions* 10.

Nemani, R. R., Keeling, C. D., Hashimoto, H., Jolly, W. M., Piper, S. C., Tucker, C. J., Myneni, R. B., and Running, S. W. (2003). Climate-driven increases in global terrestrial net primary production from 1982 to 1999. *Science* 300, 1560–1563.

Niu, S., Xing, X., Zhang, Z., Xia, J., Zhou, X., Song, B., Li, L., and Wan, S. (2011). Water-use efficiency in response to climate change: from leaf to ecosystem in a temperate steppe. *Global Change Biology* 17, 1073–1082.

Oren, R, Sperry, J., Katul, G., Pataki, D., Ewers, B., Phillips, N, and Schäfer, K. (1999). Survey and synthesis of intra-and interspecific variation in stomatal sensitivity to vapour pressure deficit. *Plant, Cell & Environment* 22, 1515–1526.

Papale, D, Reichstein, M, Canfora, E, Aubinet, M, Bernhofer, C, Longdoz, B, Kutsch, W, Rambal, S, Valentini, R, Vesala, T, et al. (2006). Towards a more harmonized processing of eddy covariance CO 2 fluxes: algorithms and uncertainty estimation. *Biogeosciences Discussions* 3, 961–992.

Papale, D. (2012). Data Gap Filling. In: *Eddy Covariance*. Springer, 159–172.

Parry, M. A., Andralojc, P. J., Khan, S., Lea, P. J., and Keys, A. J. (2002). Rubisco activity: effects of drought stress. *Annals of Botany* 89, 833–839.

Pereira, J., Mateus, J., Aires, L., Pita, G, Pio, C, David, J., Andrade, V, Banza, J, David, T., Paço, T., et al. (2007). Net ecosystem carbon exchange in three contrasting Mediterranean ecosystems? The effect of drought. *Biogeosciences* 4, 791–802.

R Core Team (2013). *R: A Language and Environment for Statistical Computing*. R Foundation for Statistical Computing. Vienna, Austria. URL: http://www.R-project.org/.

Raddatz, T., Reick, C., Knorr, W., Kattge, J., Roeckner, E, Schnur, R., Schnitzler, K.-G., Wetzel, P, and Jungclaus, J (2007). Will the tropical land biosphere dominate the climate–carbon cycle feedback during the twenty-first century? *Climate Dynamics* 29, 565–574.

Rebmann, C, Anthoni, P, Falge, E, Göckede, M, Mangold, A, Subke, J.-A., Thomas, C, Wichura, B, Schulze, E.-D., Tenhunen, J., et al. (2004). Carbon budget of a spruce forest ecosystem. In: *Biogeochemistry of Forested Catchments in a Changing Environment*. Springer, 143–159.

Rebmann, C, Göckede, M, Foken, T., Aubinet, M., Aurela, M, Berbigier, P, Bernhofer, C, Buchmann, N, Carrara, A, Cescatti, A, et al. (2005). Quality analysis applied on eddy covariance measurements at complex forest sites using footprint modelling. *Theoretical and Applied Climatology* 80, 121–141.

Reichstein, M., Falge, E., Baldocchi, D., Papale, D., Aubinet, M., Berbigier, P., Bernhofer, C., Buchmann, N., Gilmanov, T., Granier, A., et al. (2005). On the separation of net ecosystem exchange into assimilation and ecosystem respiration: review and improved algorithm. *Global Change Biology* 11, 1424–1439.

Reick, C., Raddatz, T, Brovkin, V, and Gayler, V (2013). Representation of natural and anthropogenic land cover change in MPI-ESM. *Journal of Advances in Modeling Earth Systems* 5, 459–482.

Richardson, A. D., Aubinet, M., Barr, A. G., Hollinger, D. Y., Ibrom, A., Lasslop, G., and Reichstein, M. (2012). Uncertainty quantification. In: *Eddy Covariance*. Springer, 173–209.

Rind, D., Goldberg, R, Hansen, J, Rosenzweig, C., and Ruedy, R (1990). Potential evapotranspiration and the likelihood of future drought. *Journal of Geophysical Research-Atmosphere* 95, 9983–10004.

Roeckner, E et al. (2003). The atmospheric general circulation model ECHAM5. Part I: Model description. *MPI Rep., Max Planck Inst. for Meteorol., Hamburg, Germany* 349, 127.

Roupsard, O., Bonnefond, J.-M., Irvine, M., Berbigier, P., Nouvellon, Y., Dauzat, J., Taga, S., Hamel, O., Jourdan, C., Saint-André, L., et al. (2006). Partitioning energy and evapo-transpiration above and below a tropical palm canopy. *Agricultural and Forest Meteorology* 139, 252–268.

Santiago, L., Goldstein, G, Meinzer, F., Fisher, J., Machado, K, Woodruff, D, and Jones, T (2004). Leaf photosynthetic traits scale with hydraulic conductivity and wood density in Panamanian forest canopy trees. *Oecologia* 140, 543–550.

Sanz, M., Carrara, A, Gimeno, C, Bucher, A, and Lopez, R (2004). Effects of a dry and warm summer conditions on CO_2 and Energy fluxes from three Mediterranean ecosystems. In: *Geophysical Research Abstracts*. Vol. 6, 3239–3239.

Scherer-Lorenzen, M., Schulze, E.-D., Don, A., Schumacher, J., and Weller, E. (2007). Exploring the functional significance of forest diversity: a new long-term experiment with temperate tree species (BIOTREE). *Perspectives in Plant Ecology, Evolution and Systematics* 9, 53–70.

Schmid, H. P., Grimmond, C. S. B., Cropley, F., Offerle, B., and Su, H.-B. (2000). Measurements of CO_2 and energy fluxes over a mixed hardwood forest in the mid-western United States. *Agricultural and Forest Meteorology* 103, 357–374.

Schmider, E., Ziegler, M., Danay, E., Beyer, L., and Bühner, M. (2010). Is it really robust? Reinvestigating the robustness of ANOVA against violations of the normal distribution assumption. *Methodology: European Journal of Research Methods for the Behavioral and Social Sciences* 6, 147.

Schneck, R., Reick, C. H., and Raddatz, T. (2013). Land contribution to natural CO_2 variability on time scales of centuries. *Journal of Advances in Modeling Earth Systems* 5, 354–365.

Schulze, E. (1986). Carbon dioxide and water vapor exchange in response to drought in the atmosphere and in the soil. *Annual Review of Plant Physiology* 37, 247–274.

Scott, R. L., Jenerette, G. D., Potts, D. L., and Huxman, T. E. (2009). Effects of seasonal drought on net carbon dioxide exchange from a woody-plant-encroached semiarid grassland. *Journal of Geophysical Research-Biogeosciences* 114.

Sellers, P., Bounoua, L, Collatz, G., Randall, D., Dazlich, D., Los, S., Berry, J., Fung, I, Tucker, C., Field, C., et al. (1996). Comparison of radiative and physiological effects of doubled atmospheric CO_2 on climate. *Science* 271, 1402–1405.

Simioni, G., Le Roux, X., Gignoux, J., and Walcroft, A. S. (2004). Leaf gas exchange characteristics and water-and nitrogen-use efficiencies of dominant grass and tree species in a West African savanna. *Plant ecology* 173, 233–246.

Sperry, J., Adler, F., Campbell, G., and Comstock, J. (1998). Limitation of plant water use by rhizosphere and xylem conductance: results from a model. *Plant, Cell & Environment* 21, 347–359.

Sulman, B., Desai, A., Cook, B., Saliendra, N, and Mackay, D. (2009). Contrasting carbon dioxide fluxes between a drying shrub wetland in Northern Wisconsin, USA, and nearby forests. *Biogeosciences* 6, 1115–1126.

Suni, T., Rinne, J., Reissell, A., Altimir, N., Keronen, P., Rannik, U, Maso, M., Kulmala, M., and Vesala, T. (2003). Long-term measurements of surface fluxes above a Scots pine forest in Hyytiala, southern Finland, 1996-2001. *Boreal Environment Research* 8, 287–302.

Tedeschi, V., Rey, A., Manca, G., Valentini, R., Jarvis, P. G., and Borghetti, M. (2006). Soil respiration in a Mediterranean oak forest at different developmental stages after coppicing. *Global Change Biology* 12, 110–121.

Tirone, G, Dore, S, Matteucci, G, Greco, S, and Valentini, R (2003). Evergreen Mediterranean forests. carbon and water fluxes, balances, ecological and ecophysiological determinants. In: *Fluxes of carbon, water and energy of European forests*. Springer, 125–149.

Tuzet, A, Perrier, A, and Leuning, R (2003). A coupled model of stomatal conductance, photosynthesis and transpiration. *Plant, Cell & Environment* 26, 1097–1116.

Tyree, M. T. and Ewers, F. W. (1991). The hydraulic architecture of trees and other woody plants. *New Phytologist* 119, 345–360.

Urbanski, S, Barford, C, Wofsy, S, Kucharik, C, Pyle, E, Budney, J, McKain, K, Fitzjarrald, D, Czikowsky, M, and Munger, J. (2007). Factors controlling CO2 exchange on timescales from hourly to decadal at Harvard Forest. *Journal of Geophysical Research-Biogeosciences* 112, G02020.

Valentini, R., Gamon, J. A., and Field, C. B. (1995). Ecosystem gas exchange in a California grassland: seasonal patterns and implications for scaling. *Ecology* 76, 1940–1952.

Vargas, R., Sonnentag, O., Abramowitz, G., Carrara, A., Chen, J. M., Ciais, P., Correia, A., Keenan, T. F., Kobayashi, H., Ourcival, J.-M., et al. (2013). Drought Influences the Accuracy of Simulated Ecosystem Fluxes: A Model-Data Meta-analysis for Mediterranean Oak Woodlands. *Ecosystems* 16, 749–764.

Veenendaal, E. M., Kolle, O., and Lloyd, J. (2004). Seasonal variation in energy fluxes and carbon dioxide exchange for a broad-leaved semi-arid savanna (Mopane woodland) in Southern Africa. *Global Change Biology* 10, 318–328.

Williams, M, Richardson, A., Reichstein, M, Stoy, P., Peylin, P, Verbeeck, H, Carvalhais, N, Jung, M, Hollinger, D., Kattge, J, et al. (2009). Improving land surface models with FLUXNET data. *Biogeosciences* 6, 1341–1359.

Wilson, T. and Meyers, T. (2007). Determining vegetation indices from solar and photosynthetically active radiation fluxes. *Agricultural and Forest Meteorology* 144, 160–179.

Wohlfahrt, G., Anderson-Dunn, M., Bahn, M., Balzarolo, M., Berninger, F., Campbell, C., Carrara, A., Cescatti, A., Christensen, T., Dore, S., et al. (2008a). Biotic, Abiotic, and Management Controls on the Net Ecosystem CO_2 Exchange of European Mountain Grassland Ecosystems. *Ecosystems* 11, 1338–1351.

Wohlfahrt, G., Hammerle, A., Haslwanter, A., Bahn, M., Tappeiner, U., and Cernusca, A. (2008b). Seasonal and inter-annual variability of the net ecosystem CO_2 exchange of a temperate mountain grassland: Effects of weather and management. *Journal of Geophysical Research-Atmospheres* 113.

Wong, S., Cowan, I., and Farquhar, G. (1979). Stomatal conductance correlates with photosynthetic capacity. *Nature* 282, 424–426.

Xu, L. and Baldocchi, D. D. (2003). Seasonal trends in photosynthetic parameters and stomatal conductance of blue oak (Quercus douglasii) under prolonged summer drought and high temperature. *Tree Physiology* 23, 865–877.

Zhao, M. and Running, S. W. (2010). Drought-induced reduction in global terrestrial net primary production from 2000 through 2009. *Science* 329, 940–943.

Zhou, S., Duursma, R. A., Medlyn, B. E., Kelly, J. W., and Prentice, I. C. (2013). How should we model plant responses to drought? An analysis of stomatal and non-stomatal responses to water stress. *Agricultural and Forest Meteorology* 182, 204–214.

Zimmermann, M. H. (1978). Hydraulic architecture of some diffuse-porous trees. *Canadian Journal of Botany* 56, 2286–2295.

Appendices

A C4 photosynthesis

For C4 photosynthesis, Eqs. 1-3 are replaced by the following (Collatz et al., 1992):

$$A_n = \min(J_c; J_e) - R_d \tag{A.1}$$

$$J_c = k_s\, C_i \tag{A.2}$$

$$J_e = \frac{1}{2\Theta_s}\left(V_{pmax} + J_i - \sqrt{(V_{pmax} + J_i)^2 - 4\Theta_s V_{pmax} J_i}\right) \tag{A.3}$$

where k_s represents the PEPcase CO_2 specificity, Θ_s is a curvature parameter for J_e, and V_{pmax} is the maximum PEP carboxylation rate. The light limited assimilation rate J_i depends on photosynthetically active radiation. For details see Collatz et al. (1992).

B Temperature response of photosynthesis

As the temperature functions in the original photosynthesis model of Farquhar et al. (1980) are based on *in vitro* measurements over a limited temperature range (Farquhar et al., 1980; Bernacchi et al., 2001), temperature functions of the Michaelis-Menten constants for CO_2 (K_c) and O_2 (K_o) were revised according to Bernacchi et al. (2001), who estimated Rubisco kinetic properties *in vivo* over a wide range of temperatures, CO_2, and O_2 concentrations. The formulations of the temperature response functions for K_c and K_o remain unaltered, but the parameter values were revised (Tab. B1):

$$K_c = K_{c,0}\ \exp\left(\frac{E_c(T_v - 298.15)}{RT_v 298.15}\right) \tag{B.1}$$

$$K_o = K_{o,0}\ \exp\left(\frac{E_o(T_v - 298.15)}{RT_v 298.15}\right) \tag{B.2}$$

where $K_{c,0}$ and $K_{o,0}$ are the corresponding Michaelis-Menten values for CO_2 and O_2, respectively, at the reference temperature of 25°C, E_c is the activation energy for K_c, E_o is the activation energy for K_o, and T_v is the vegetation temperature. The revised parameter values and corresponding units can be extracted from Tab. B1.

In previous model versions, the temperature response of the CO_2 compensation point in the absence of dark respiration (Γ^*) was assumed to be linear (Farquhar, 1988), but Bernacchi et al. (2001) proposed an exponential increase with temperature:

$$\Gamma^* = \Gamma^*_0\ \exp\left(\frac{E_g(T_v - 298.15)}{RT_v 298.15}\right) \tag{B.3}$$

where Γ^*_0 is the value of Γ^* at the reference temperature of 25°C, and E_g is the activation energy for Γ^*. The previous and revised response functions are shown in Fig. B1.

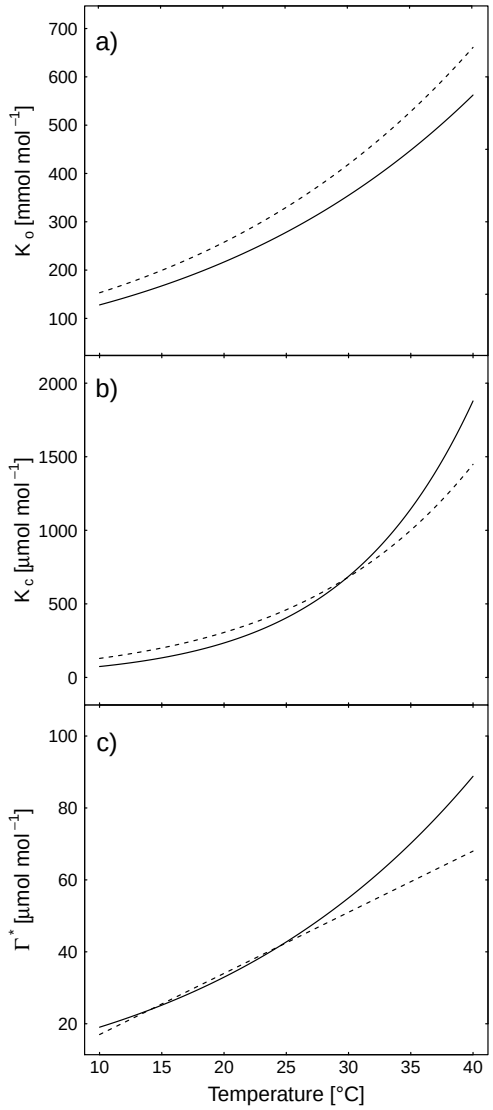

Fig. B1. Revised temperature responses of (a) K_o, (b) K_c, and (c) Γ^* from Bernacchi et al. (2001) (solid line) compared to the original functions from Farquhar et al. (1980)(dashed line).

Tab. B1. Previous and revised parameter values for K_c, K_o, and Γ^*

	Value at 25°C		activation energy [kJ mol^{-1}]	
Parameter	previous[a]	revised[b]	previous[a]	revised[b]
K_c[μmol mol^{-1}]	460.00	404.90	59.36	79.43
K_o[mmol mol^{-1}]	330.00	278.40	35.95	36.38
Γ^*[μmol mol^{-1}]	-	42.75	-	37.83

[a] according to Farquhar et al. (1980)

[b] according to Bernacchi et al. (2001)

C Adjustment of photosynthetic capacity

For the site-level runs, photosynthetic capacity was adjusted to conditions at the respective FLUXNET site. Since the different model versions presume different C_i/C_a ratios with effects on productivity, the adjustment was performed for each model version. The adjustment was based on light-response curves (Fig. C1). Half-hourly GPP-data derived from eddy-covariance measurements and simulated net assimilation values under favorable conditions for photosynthesis (VPD $<$ 1 kPa, Temperature $>$ 15°C, no soil water stress) were plotted against radiation, and the median was calculated for both observed and simulated values $>$ 1500 μmol m^{-2} s^{-1}. V_{cmax} was then changed according to the ratio of the two medians. J_{max} was changed proportionally to V_{cmax} assuming a constant relation $J_{max} = 1.9V_{cmax}$ for C3 plants and $k_s = 10V_{pmax}$ for C4 plants.

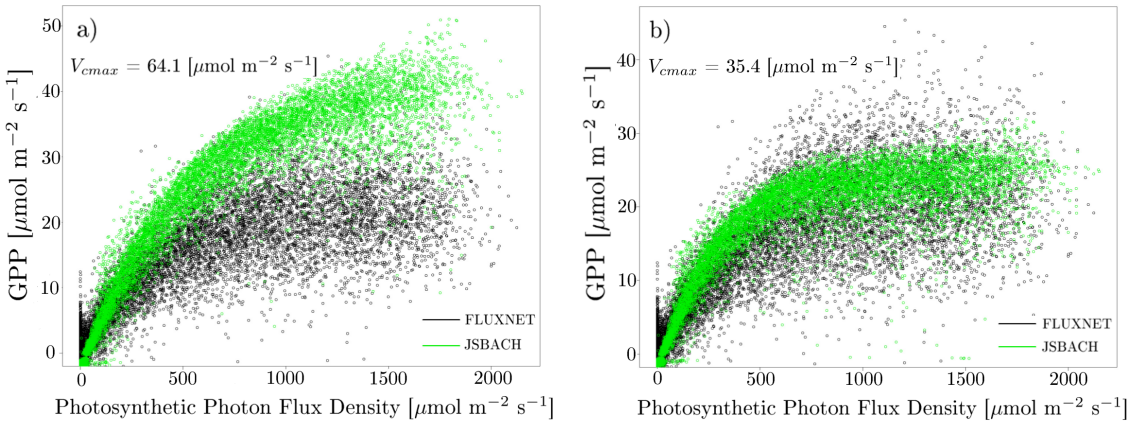

Fig. C1. Light response curves for the station DE-Tha, a coniferous evergreen forest (a) before and (b) after the adjustment of V_{cmax} and J_{max}, shown for the Ball-Berry model version.

D Flux data filtering

D.1 Growing season filter

Growing season was delineated based on derived GPP-flux data. A site-specific GPP threshold was calculated as 20% of the 95th percentile of all daily GPP-values. Time series of daily GPP values was then smoothed using a standard moving average filter (window width = 11 days). Days of the smoothed GPP series exceeding this threshold were considered to be in the growing season if a certain number of adjacent values also exceeded the threshold (Fig. D1).

The method turned out to be robust as it considers site-specific abiotic and biotic conditions such as climate, vegetation structure and LAI, and furthermore ignores short-term variations in GPP. Thus, no adjustment was necessary for individual sites.

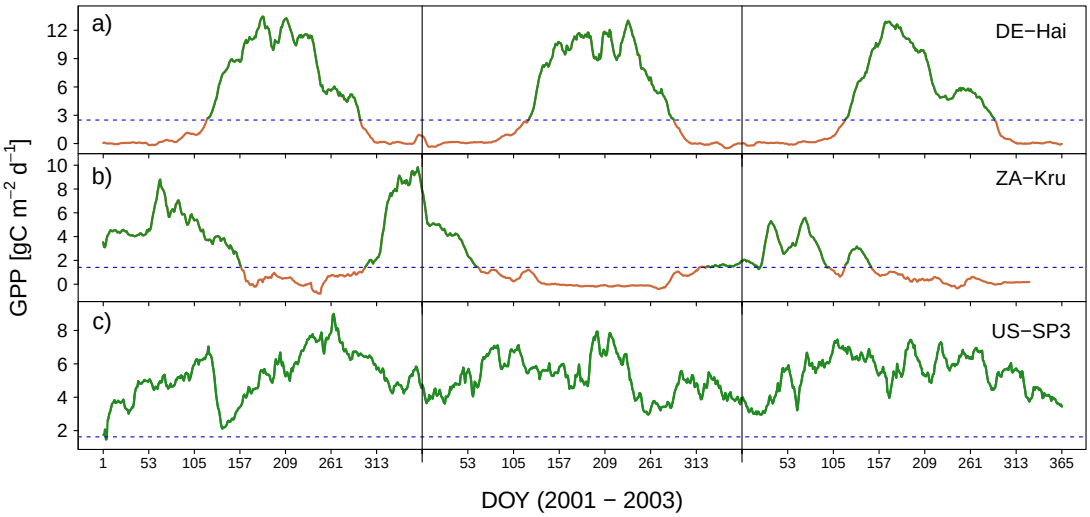

Fig. D1. Time series of smoothed daily GPP values for (a) a temperate broadleaf deciduous site (Koeppen-Geiger climate: Cfb), (b) a savanna site (Cwa), and (c) a coniferous broadleaf evergreen site (Cfa). Green lines depict time periods in the growing season, and brown lines represent time periods outside the growing season. The blue dashed line indicates the GPP-threshold calculated as 20% of the 95th percentile of the daily GPP values.

D.2 Soil water stress filter

Since in this study the focus lied on non-water-stressed conditions, flux data recorded under water stressed conditions were excluded for most parts of the analyses. The underlying assumption for the filtering procedure described in this section was that the effect of soil moisture stress becomes apparent in the derived GPP data. For the filtering, the quality filtered GPP data set is split into 15 soil moisture classes of equal width and for each class the median is calculated. The threshold is defined as the first soil moisture class in which the median exceeds 95% of the mean of all higher soil moisture classes. All values exceeding the threshold were considered as unstressed with respect to soil moisture.

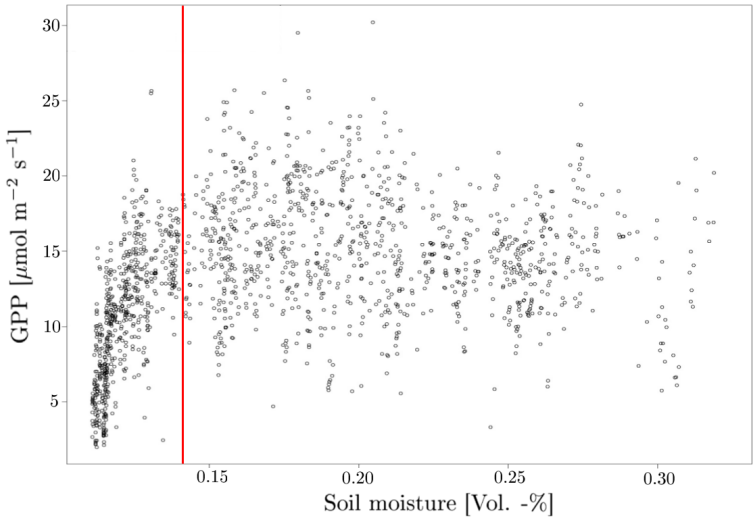

Fig. D2. GPP plotted against soil moisture for a Mediterranean station (FR-Pue). The red line indicates the threshold below which values were considered as water-stressed.

E Derivation of aerodynamic conductance and intercellular CO_2 concentration

The derivation of aerodynamic conductance G_a in this study requires the transfer coefficients for heat (C_h) and momentum (drag coefficient C_D). G_a is then related to C_h as shown in Eq. E.6. Transfer coefficients were calculated based on the Monin-Obukhov similarity theory, which states that the mean vertical gradient of a scalar is, if appropriately scaled, a unique function of a stability parameter (Bonan, 2008, p.208). Besides atmospheric stability, transfer coefficients depend on surface roughness. The drag coefficient for neutral stability (C_{DN}) is given by:

$$C_{DN} = \frac{k^2}{\ln((z_s - d)/z_0)^2} \tag{E.1}$$

where $k = 0.41$ is the von-Kármán constant, z_s is the vegetation height, d is the zero-plane displacement height, and z_0 is the roughness length, which was assumed to be proportional to the vegetation height with $z_0 = 0.125 z_s$. Vegetation height was either reported for individual FLUXNET sites in the ancillary database or set to a PFT-specific default value (Tab. 1). The zero-plane displacement height is calculated from the logarithmic wind profile equation:

$$d = z_s - z_0 \exp(uk/u*) \tag{E.2}$$

where u is horizontal wind velocity, and u_* is friction velocity. To determine the stratification in the atmosphere, the bulk Richardson number was calculated:

$$Ri_b = \frac{g(z_s - d)(T_s - T_g)}{T_g u^2} \tag{E.3}$$

where g is gravitational acceleration, T_s is potential air temperature at canopy height, and T_g is potential ground temperature. The dimensionless heat transfer coefficient C_h is calculated using analytic approximations according to Hansen et al. (1983):

$$\begin{aligned} D_M &= \sqrt{\frac{(1 - a\,Ri_b)(1 - b\,Ri_b)}{1 - c\,Ri_b}} \\ C_D &= D_M \cdot C_{DN} \\ C_h &= C_D 1.35 \sqrt{\frac{(1 - d\,Ri_b)}{(1 - f\,Ri_b)}} \end{aligned} \tag{E.4}$$

in case of an unstable stratification (i.e. $Ri_b < 0$) and as

$$\begin{aligned} D_M &= \frac{1}{1 + (11.2 + 90 Ri_b) Ri_b} \\ C_D &= D_M \cdot C_{DN} \\ C_h &= C_D 1.35/(1 + 1.93 Ri_b) \end{aligned} \tag{E.5}$$

in case of a stable stratification (i.e. $Ri_b > 0$). D_M gives the variation of drag coefficient in conditions of non-neutral stability. The coefficients in Eq. E.4 are taken from Hansen et al. (1983). Aerodynamic conductance is finally given by:

$$G_a = C_h u \tag{E.6}$$

The canopy-scale intercellular CO_2 concentration C_i is given by:

$$C_i = C_a - GPP\frac{1.42}{G_c} + \frac{1.65}{G_a} \tag{E.7}$$

where the two constants serve to convert resistance units from water to CO_2 according to Monteith (1973).

F Decoupling coefficient Ω

The decoupling coefficient Ω (Jarvis, 1986) describes the similarity between meteorological conditions at the vegetation surface and in the free atmosphere. Ω ranges between 0 and 1. Values near 0 indicate well coupled conditions and high physiological control of water and carbon fluxes. The coefficient is given by (Jarvis, 1986):

$$\Omega = \frac{\epsilon + 1}{\epsilon + 1 + G_a/G_s} \tag{F.1}$$

where ϵ is the change of latent heat content relative to the change of sensible heat content of saturated air, and G_a is the aerodynamic conductance as calculated in Appendix E. Ω was calculated based on daylight values for all sites on a half-hourly basis.

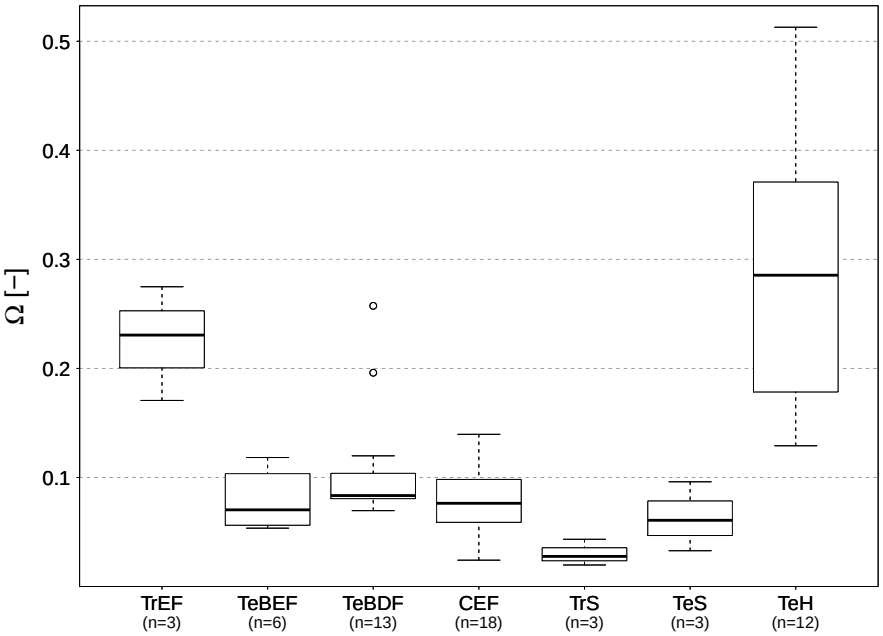

Fig. F1. Decoupling coefficient Ω calculated for different PFTs. Shown are box plots of site medians which were calculated based on half-hourly values.

G Estimation of the slope parameter g_1 from flux data

The slope parameter g_1 in the Ball-Berry model and the USM was estimated from eddy covariance data. The slope was obtained from linear least square regression, i.e. derived G_c data were regressed against $\frac{GPP \cdot h}{C_a}$ for the Ball-Berry model and against $\frac{GPP}{C_a\sqrt{VPD}}$ for the USM. Prior to the regression procedure, GPP data were aggregated to 3-hourly means, and values were removed when mean air temperature $< 10°C$ and VPD < 0.2 kPa. Moreover, only daytime GPP data within the growing season and in the absence of soil water stress were used.

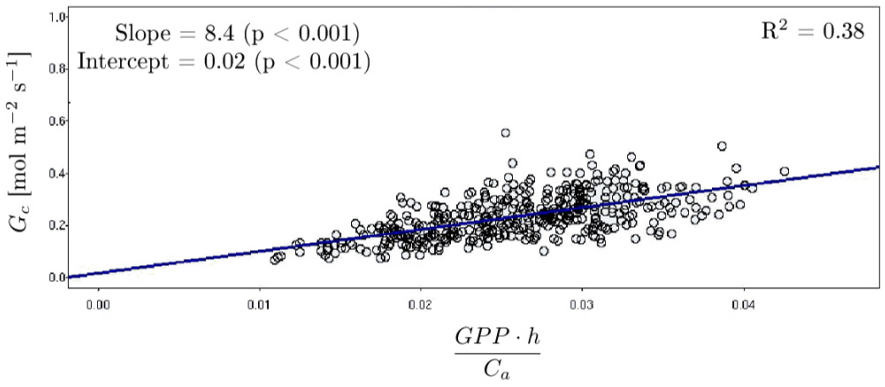

Fig. G1. Example of a linear least square regression to estimate intercept (representing g_0) and slope (representing g_1) from eddy covariance data for the Ball-Berry model. Data are shown for the station BE-Bra, a mixed forest in Western Europe.

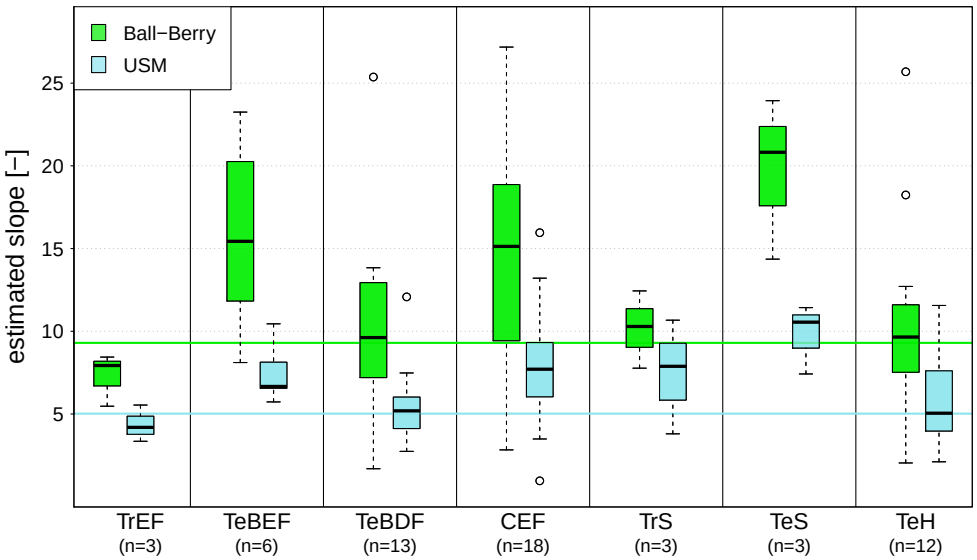

Fig. G2. Estimated slopes (representing parameter g_1 for the Ball-Berry model and the USM). Colored lines indicate the parameter values currently used in the model (Ball-Berry: 9.3, USM: 5.0).

H Mean annual course of ET and GPP for a Mediterranean site

The annual course of GPP and ET of a Mediterranean station (FR-Pue) subject to summer drought is depicted in Fig. H1. The station illustrates the differences between the models over the course of a year. Higher water use due to higher G_c in the spring leads to lower transpiration and GPP in the summer in the standard model, whereas lower G_c in the early growing season enhances transpiration and productivity during the summer drought in the alternative models.

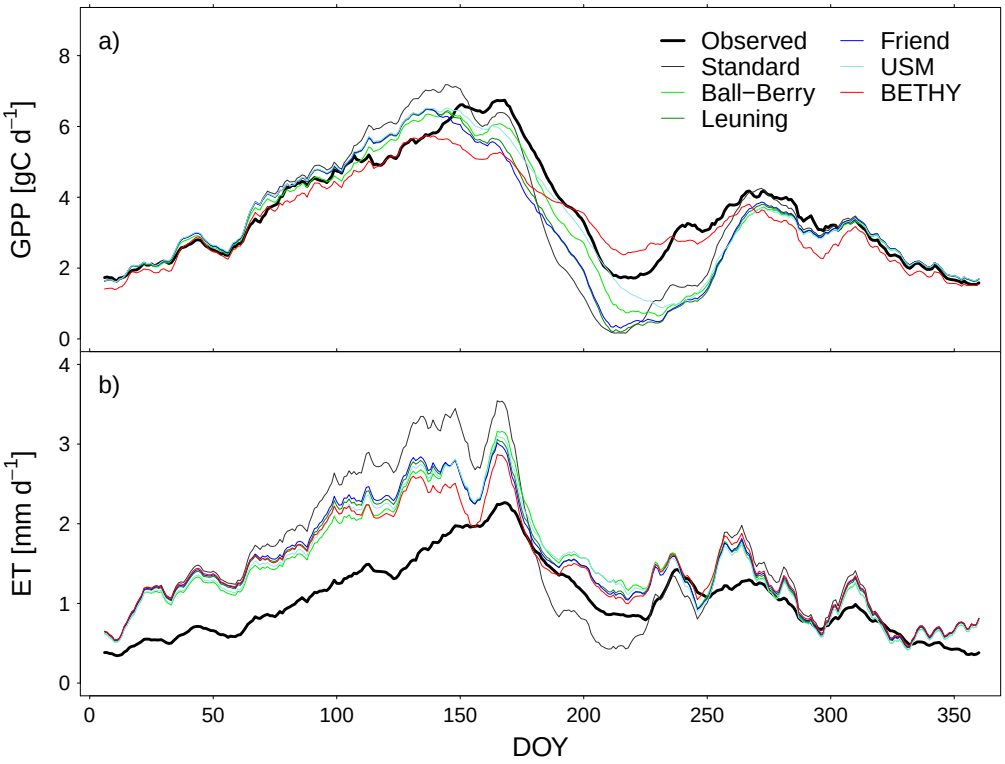

Fig. H1. Mean annual course of (a) GPP and (b) ET for a Mediterranean station, averaged over the time period 2001-2006. Shown are daily means smoothed by a moving average filter (window width = 11 days).

Erklärung

Hiermit erkläre ich, dass ich diese Masterarbeit selbständig verfasst und keine anderen als die angegebenen Quellen und Hilfsmittel benutzt habe. Die Arbeit wurde keinem anderen Prüfungsamt in gleicher oder vergleichbarer Form vorgelegt und wurde nicht veröffentlicht.

Ort und Datum	Unterschrift